NRL Report 8458

The Aging of Cork-Rubber Decoupling Materials

L. E. Horsley and C. M. Thompson

Transducer Branch
Underwater Sound Reference Detachment
P.O. Box 8337
Orlando, FL 32856

March 9, 1981

NAVAL RESEARCH LABORATORY
Washington, D.C.

SECURITY CLASSIFICATION OF THIS PAGE *(When Data Entered)*

REPORT DOCUMENTATION PAGE		READ INSTRUCTIONS BEFORE COMPLETING FORM
1. REPORT NUMBER NRL Report 8458	2. GOVT ACCESSION NO.	3. RECIPIENT'S CATALOG NUMBER
4. TITLE *(and Subtitle)* THE AGING OF CORK-RUBBER DECOUPLING MATERIALS		5. TYPE OF REPORT & PERIOD COVERED Interim report on a continuing problem. 6. PERFORMING ORG. REPORT NUMBER
7. AUTHOR(s) L. E. Horsley* and C. M. Thompson		8. CONTRACT OR GRANT NUMBER(s)
9. PERFORMING ORGANIZATION NAME AND ADDRESS Underwater Sound Reference Detachment Naval Research Laboratory PO Box 8337, Orlando, FL 32856		10. PROGRAM ELEMENT, PROJECT, TASK AREA & WORK UNIT NUMBERS 64503N S0219-AS 59-0584-0
11. CONTROLLING OFFICE NAME AND ADDRESS Naval Sea Systems Command (SEA63X5-1) Washington, DC 20362		12. REPORT DATE March 9, 1981 13. NUMBER OF PAGES 51
14. MONITORING AGENCY NAME & ADDRESS*(if different from Controlling Office)*		15. SECURITY CLASS. *(of this report)* UNCLASSIFIED 15a. DECLASSIFICATION/DOWNGRADING SCHEDULE

16. DISTRIBUTION STATEMENT *(of this Report)*

Approved for public release; distribution unlimited.

17. DISTRIBUTION STATEMENT *(of the abstract entered in Block 20, if different from Report)*

18. SUPPLEMENTARY NOTES

*Current address: Tactical Analysis Division, U.S. Naval Oceanographic Office, NSTL Station, MS 39522.

Part of this report was previously published as Mr. Horsley's Master's Thesis at the Florida Institute of Technology, dated June 1980.

19. KEY WORDS *(Continue on reverse side if necessary and identify by block number)*

Sonar transducers	Sound speed
Fill fluids	Attenuation
Acoustic decouplers	Hydrophone
Permeation	Acoustic impedance

20. ABSTRACT *(Continue on reverse side if necessary and identify by block number)*

Pressure-release materials are used to insulate some components of sonar transducers. By acoustically shielding some areas of the transducer, the directivity and sensitivity can be greatly altered.

Pressure-release materials insulate because of their large differences in acoustic impedance from that of the other components and fluids used in transducers. One serious problem is that these pressure-release materials absorb the transducer fill fluids. This increases the acoustic impedance and therefore reduces the effectiveness of the acoustic insulation.

(Continued)

20. Abstract (Continued)

The absorption mechanism is investigated by microscopic analysis, gravimetric analysis, and microtome sectioning. An explanation of the fluid permeation mechanism is offered along with the time-temperature dependence. Resulting changes in the acoustic properties with fluid absorption are studied using an acoustic impedance tube and G19 hydrophone calibrator. An equation is formulated to predict the changes in sensitivity of a simple hydrophone resulting from aging of its pressure-release material.

CONTENTS

THE AGING OF CORK-RUBBER DECOUPLING MATERIALS

INTRODUCTION

Sonar transducers must be reliable, precise, and relatively service free for reasons of safety (for both men and equipment), mission, and cost control. Therefore, the materials used to construct transducers must be compatible with both the underwater environment and the other materials within the transducer. In general the problem of material compatibility within the transducer, and more specifically the rate at which transducer fill fluids are absorbed by pressure-release materials and the effect this fluid absorption has on transducer operation and reliability, is the concern of this investigation.

Acoustic decoupling or pressure-release materials are used to acoustically insulate some components of sonar transducers. By acoustically shielding some areas of the transducer and/or isolating others, the directivity and sensitivity can be significantly altered. The pressure-release material is often wrapped around a piezoelectric ceramic element to shield the sides of the element from sound-pressure waves (Fig. 1) or to acoustically decouple a ceramic element from other internal transducer components (Fig. 2). For pressure-release materials to be effective their specific acoustic impedance must be very different from that of the fluid in which the sound-pressure wave is traveling and with which the transducer is filled.

The most commonly used pressure-release material has been Armstrong Cork Company type DC-100 corprene, a cork-neoprene-rubber composite manufactured for use as a gasket material. Armstrong claims that the DC-100 is unaffected by exposure to vegetable oil [1]. Tests have shown that DC-100 corprene can actually absorb over 50% of its own weight in castor oil, the most widely used transducer fill fluid. The absorbed fluid increases the specific acoustic impedance of the decoupling material and, thereby, reduces the impedance mismatch. This reduction in mismatch reduces the acoustic insulating ability of the material which, in turn, alters the sensitivity and directivity of the transducer. This means that whether the transducer is in active service or is still in storage, its acoustic properties are slowly changing with time. To date, no method exists for

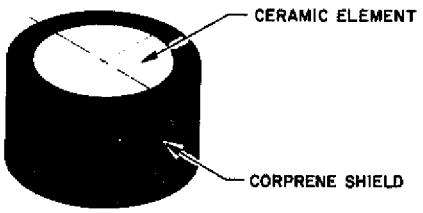

Fig. 1 — Ceramic element radially shielded with corprene

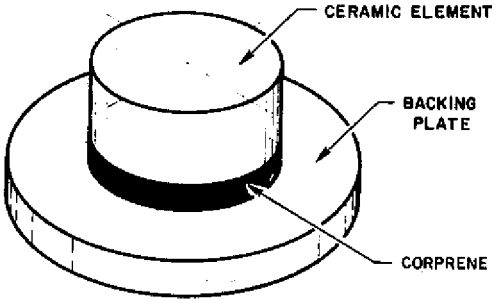

Fig. 2 — Ceramic element decoupled from its backing plate by using corprene

Manuscript submitted September 30, 1980.

compensating for the changes without taking the transducer out of service for recalibration and/or rebuilding.

The problem with corprene has existed, at least to some extent, since the early 1940's. The Red Books of World War II [2] mention the need for replacement of corprene in pressure-release applications. Although it has been a long-standing problem, very little information can be found in the literature dealing with testing and modeling of pressure-release materials. Higgs and Eriksson [3] investigated the acoustical changes in precompressed onionskin paper with changes in temperature and pressure. Higgs, D'Amico, and Speerschneider [4] studied the pressure dependence of sonite, but neither of the aforementioned reports included any aging effects.

Literature specifically discussing DC-100 corprene is even more restricted. Higgs and Eriksson [5] investigated the changes in DC-100 with respect to temperature and pressure; but again, no mention was made of possible changes caused by castor-oil absorption.

Two reports were found that discuss the problem of oil penetration into corprene. Both were basically concerned with a single hydrophone element and had limited distribution. Robertson [6] presented a short study of castor-oil absorption in corprene utilizing extraction techniques on three samples at two temperatures. No general quantitative conclusion was reported. Fife [7] investigated the changes caused by castor-oil penetration into the space between the ceramic element and the corprene decoupler. Fife did include a short qualitative study of the castor-oil absorption problem, but he examined neither the rate of castor-oil absorption nor the effects of this absorption on a hydrophone element.

The objective of the study discussed in this report is to independently determine both the rate of oil saturation of cork-rubber composites and the changes in acoustic properties brought about by oil saturation.

THEORY

The equations-of-state of the piezoelectric medium can be derived from thermodynamic potentials. A complete treatment starting with either the Gibbs function or the Helmholtz function is done by Berlincourt, Curran, and Jaffe and can be found in Mason [8]. In this work matrix notation will be used. The simplified equations-of-state for a hydrophone with stress and electric displacement as the independent variables are given by Mason as

$$E = gT + (1/\epsilon)D \tag{1}$$

and

$$S = s^D T + g_t D\,, \tag{2}$$

where D = electric displacement,
E = electric field,
g = piezoelectric voltage constant,
g_t = transposed matrix of g,
s^D = elastic compliance,
S = strain,
T = stress,
ϵ = permittivity

for the piezoelectric ceramic elements.

Now consider a small ceramic element in the shape of a right circular cylinder with its parallel faces normal to the 3-direction (z-axis) as shown in Fig. 3. The electrodes are located on the parallel faces. If a slowly varying pressure field (acoustical signal below 1000 Hz) is chosen, the pressure can be considered as hydrostatic on all faces of a small piezoelectric ceramic at any given time since the wavelength is much greater than the ceramic element size. Therefore, the shear stresses are zero, and the normal stress components are all equal.

$$T_1 = T_2 = T_3 \ . \tag{3}$$

If the ceramic disc is polarized in the 3-direction, then the electric field is zero in the radial direction, so

$$E_1 = E_2 = 0 \ , \tag{4}$$

leaving the governing equation

$$E_3 = gT + (1/\epsilon)D. \tag{5}$$

Piezoelectric ceramics have a very high resistivity and, therefore, a very low conductivity that drives the electric displacement term to zero (proof in Appendix A). This further reduces Eq. (1) to

$$E_3 = -gT \ ; \tag{6}$$

or if written in component form,

$$E_3 = -(g_{31}T_1 + g_{32}T_2 + g_{33}T_3) \ . \tag{7}$$

Because of symmetry, the piezoelectric voltage constants are equal in the radial direction.

$$g_{13} = g_{31} = g_{32} \tag{8}$$

So, Eq. (7) can be rewritten as

$$E_3 = -(g_{31}T_1 + g_{31}T_2 + g_{33}T_3) \ , \tag{9}$$

or finally by substitution of Eq. (3) into Eq. (9) as

$$E_3 = -(2g_{31} + g_{33})T_3 \ . \tag{10}$$

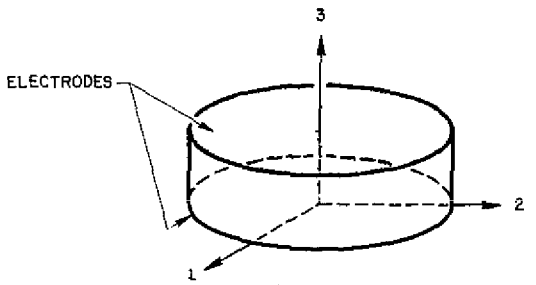

Fig. 3 — Orientation of ceramic disc

Since the stress is actually the acoustic pressure and the electric field is the voltage divided by the distance between the electrodes, Eq. (10) becomes

$$E_3 = V/x = -(2g_{31} + g_{33})p \; ; \tag{11}$$

where p = acoustic pressure, V = voltage, and x = distance between electrodes; or in the final working form,

$$M \equiv V/p = (2g_{31} + g_{33})x \; , \tag{12}$$

where M is the free field voltage sensitivity.

The voltage sensitivity shall be examined to find the theoretical difference between an unshielded ceramic element (Case 1) and a radially shielded ceramic element (Case 2). The values of the piezoelectric voltage constants for PZT-4 (Trademark of Clevite Corp.)—the most commonly used lead titanate zirconate ceramic—are given by Mason [8] to be $g_{31} = -0.0111$ *Vm/N* and $g_{33} = 0.0261$ *Vm/N*.

Case 1: Acoustic pressure is acting equally on all faces of the ceramic disc, so the voltage sensitivity is

$M = (2g_{31} + g_{33})x$,
$M = [2(-0.0111) + 0.0261]x$, and
$M = 0.0039x$.

Case 2: Acoustic pressure is shielded radially so

$T_1 = T_2 = 0$ and
$T_3 \neq 0$.

Substituting this into Eq. (7) leaves $E_3 = g_{33}T_3$, or in terms of voltage sensitivity, $M = g_{33}x$ and $M = 0.0261x$. The value of the voltage sensitivity for the second case is over six times the value of the voltage sensitivity of the first case.

Corprene is neither a perfect acoustic insulator (i.e., Case 2) when unaffected by transducer fill fluid nor is it acoustically transparent (i.e., Case 1) when it is completely saturated. But it is apparent from the above example that transducer fill-fluid absorption by an acoustic pressure-release material can significantly affect the voltage sensitivity of a piezoelectric sonar transducer.

MATERIALS AND EQUIPMENT

The materials tested for material compatibility and for stability of acoustic properties consist of five cork-rubber composites. These include polychloroprene-cork (types DC-100 and DC-116), polynitrilebutadiene-cork (types NC-710 and NC-775), and silicone rubber-cork (type LC-800). The material specifications of these composites as given by the manufacturer, Armstrong Cork Co., are presented in Table 1. All five composites are manufactured primarily for use as gasket materials and are listed as oil resistant for this purpose.

The transducer fill fluids used for the compatibility testing are listed in Table 2 along with their manufacturer's material specifications. Castor oil (Baker Company DB grade) is the most

Table 1 — Material Specifications for Cork-Rubber Composites Tested as Given by Armstrong Cork Co.

Material	Characteristics and Uses	Type	Specific Gravity (maximum)	Hardness (Shore Type A)	Compressibility (%)	Price per sheet 1/8″ X 36″ X 36″ (in 1978)
DC-100	General-purpose gasket and sealing material; high cork content, minimum side flow.	Cork and neoprene (polychloroprene)	0.90	55-70	20-30 (300 psi)	$12.95
DC-116	Like DC-100, but higher density.	Cork and neoprene (polychloroprene)	—	60-75	20-35 (400 psi)	$15.85
NC-710	Like DC-100, but with maximum oil and solvent resistance.	Cork and nitrile-butadiene rubber	0.90	55-70	20-30 (300 psi)	$12.80
NC-775	High quality, excellent resistance to transformer oils.	Cork and nitrile-butadiene rubber	—	70-85	10-25	$24.00
LC-800	Outstanding flexibility and resilience over wide range of temperatures.	Cork and silicone rubber	1.15	63-77	10-25 (300 psi)	$70.00

Table 2 — Material Specifications for Transducer Fill Fluids Tested at 25°C for Material Compatibility with Cork-Rubber Composites

Name	Manufacturer	Chemical Description	Density (kg/m^3)	Viscosity (cs)	Sound speed (m/s)
Castor Oil	Baker Company DB grade	glycerol (triricinoleate)	959	825	1507
Silicone Oil	Dow Corning DC-200 Fluid	poly(dimethylsiloxane)	960	100	1073
PAG	Union Carbide LB 135Y3	monobutyl ether of polypropylene glycol	1000	52	1312

commonly used fill fluid for transducer application. Silicone oil (Dow Corning DC-200 Fluid) is currently in limited use, and monobutylether of polypropylene glycol (PAG) (Union Carbide LB 135Y3) was being tested for possible low-temperature use when this investigation was started.

Preliminary microscopic analysis was performed using a Bausch and Lomb binocular microscope with 9.9X-, 19.5X-, and 112.5X-power magnifications. The actual analysis and photography were done with a Bausch and Lomb StereoZoom 4 Microscope with continuous magnification from 10.5X to 45.0X power.

Weighing for all test samples was done with a Mettler H311 Balance.

Sectioning for tests on depth-of-oil penetration was done with an American Optical Company Model 900 Microtome. In conjunction with the sectioning, preliminary infrared spectrophotometry was done on a Perkin-Elmer Model 599 Spectrophotometer, utilizing multiple internal reflectance techniques, and a Perkin-Elmer Model 621 Spectrophotometer was used for research.

The acoustic impedance tube and accompanying electronics are a custom-made system. A detailed discussion of the system (excluding updated electronics) can be found in the article by Sabin [9].

A USRD type G19 hydrophone calibrator was used to test the effects of oil permeation on an active PZT-4 piezoelectric ceramic element. A USRD standard F61 hydrophone was used as the comparison standard for these tests [10].

EXPERIMENTAL PROCEDURE

The first part of this investigation employed methods from physical chemistry to determine the rate of absorption of transducer fill fluids by the pressure-release materials and the speed-of-advance of the fluid front. This was accomplished with the aid of three separate techniques: microscopic analysis, gravimetric analysis, and thin-layer sectioning. Testing procedures from physical acoustics were then used to determine the effects of transducer fill-fluid absorption on the acoustic properties of the materials being tested, and in turn to determine how these changes affect an active piezoelectric ceramic element. This was accomplished by studying materials in an acoustic impedance tube and testing a wrapped PZT-4 ceramic element in the G19 hydrophone calibrator.

Microscopic Analysis

Microscopic analysis was conducted to obtain an understanding of the oil-permeation problem by visual means. Preliminary work was done using a Bausch and Lomb binocular microscope. In this preliminary research, castor-oil-soaked DC-100 composite was sectioned parallel to the direction of oil penetration and studied at 9.9X-, 19.5X-, and 112.5X-power magnifications. Several common dyes (including methyl red, phenol red, methylene blue, and bromothymol blue) were mixed with castor oil using a heated magnetic stirrer in an attempt to enhance the color of the castor oil and, therefore, make the location of the fluid front easier to track visually.

The actual analysis was performed using a Bausch and Lomb StereoZoom 4 Microscope. It was hoped that this microscope used in conjunction with a micrometer disc would make the visual tracking more quantitative. A camera adapter and Nikon 35-mm single reflex camera provided photographic recording of the castor-oil permeation.

The samples investigated were sections taken from the same samples used for the microtome sectioning. Composite types DC-100, DC-116, NC-710, and NC-775 were cut parallel to the direction of castor-oil penetration.

Gravimetric Analysis

The principal purpose of the gravimetric analysis was to determine the rate of absorption of transducer fill fluids into cork-rubber composites. Tests were conducted at 25°, 75°, and 100°C to determine the temperature dependence of the fluid permeation rate and to determine a suitable temperature to accelerate the aging process for other possible test projects. The fluids used in this series of tests were castor oil, silicone oil, and PAG; the cork-rubber composites tested were types DC-100, DC-116, NC-710, NC-775, and LC-800. Table 3 shows the combinations of fluids, composites, and temperatures that were tested. All gravimetric samples were 15 × 10 × 0.3175 cm when the tests began. By maximizing the surface-to-edge ratio, the problem could be considered as two fluid fronts converging toward the middle and edge interactions ignored. The cork-rubber samples were wiped as dry as possible before each weighing to reduce the amount of fluid adhering to the exposed surface areas. After one month, some of the samples showed evidence of change in volume and hardness. Therefore, at several times the dimensions of individual samples were measured and the hardness was tested using a Shore 2A Durometer.

Microtome Sectioning

Analysis by microtome sectioning was conducted as a method to determine the rate of change in density of the cork-rubber composites in relation to the depth of castor-oil penetration. Samples for microtome sectioning were prepared by immersing 7.72 × 3.64 × 1.27-cm blocks of DC-100, DC-116, NC-710, or NC-775 composite in castor oil. Tests were then performed at 25° and 75°C on these soaked samples, which had been sectioned perpendicular to the direction of oil permeation at 250-μm intervals.

Difficulties arose with the use of infrared spectrophotometry to monitor the castor-oil permeation. The feasibility of this method was based on spectra obtained from the different cork-rubber composites and the transducer fill fluids, and from the outer surface of the composites soaked for short periods of time in the fill fluids. The tests were conducted using multiple internal reflectance techniques. Early tests showed that a very intense absorption peak at a wave number of 1450 cm^{-1} should occur when castor oil is present that is not present in the spectra for dry DC-100. When actual tests were started, the 1450-cm^{-1} absorption peak was not well defined and no other peak

Table 3 — Combinations of Cork-Rubber Composites and Transducer Fill Fluids Tested

Cork-Rubber Material	Castor Oil	Silicone Oil	PAG
DC-100	X	X	X
DC-116	X		
NC-710	X	X	X
NC-775	X	X	
LC-800	X	X	X

All combinations shown were tested at 25°, 75°, and 100°C.

could be found of sufficient intensity for quantitative work. The problem seemed to be that the preliminary tests were conducted on samples coated with but not soaked in castor oil. This produced a spectrum of castor oil with a slight influence from the cork-rubber composites. When the actual testing was started with the sectioned samples, the spectrum was that of DC-100 with only a slight influence of castor oil. The castor-oil peaks were present but not of sufficient intensity for quantitative analysis.

The method replacing the infrared method consisted of trimming each 250-μm section to 1.4 X 3.05 cm using a template. This standardized the length and width of each section. The thicknesses of the first five sections were checked using a micrometer. They were weighed, and the density of each was calculated.

Acoustic Impedance Tube

Impedance-tube tests were conducted to determine both the acoustic characteristics of DC-100, DC-116, NC-710, NC-775, and LC-800 composites and the changes that occurred in the acoustic properties because of castor-oil absorption.

The impedance tube for this series of tests was a 180-cm-long, stainless steel tube with a 5.08-cm inside diameter and a 2.54-cm-thick wall. Normal operating frequencies are 3 to 10 kHz at pressures from 0 to 70 MPa. The impedance-tube assembly, electronics, temperature system, pressure system, and vacuum system are shown in Fig. 4.

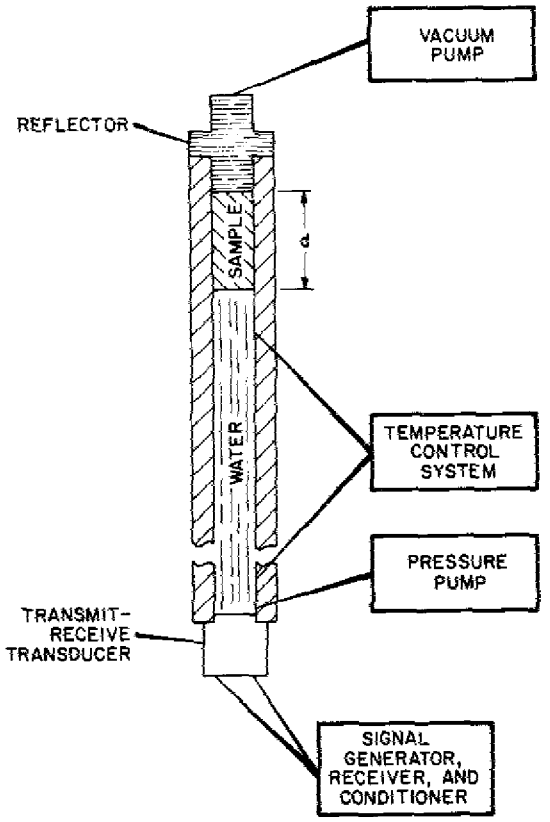

Fig. 4 — Cross section of the acoustic impedance tube used to determine sound speed and attenuation of various samples

A transducer that alternately transmits and receives a pulse of several cycles is mounted at one end of the tube. At the other end of the acoustic transmission line is a quarter-wavelength, stainless-steel reflector that provides both a termination of finite impedance and a mounting surface for the test sample.

A 1-ms coherent sinusoidal pulse is transmitted from the transducer into the acoustic transmission line. The pulse is then reflected by the reflector. Before the signal returns, the transducer is electronically switched to the receiving mode. The transducer remains in the receiving mode for several milliseconds while the pulse is reflected back and forth between the transducer and the reflector and is eventually attenuated. After a steady-state condition exists (approximately three to five reflections), the phase and amplitude of the signal are measured. The transducer is switched back to the transmitting mode and the cycle repeated. The switching takes place several hundred times per second and is averaged over many thousands of cycles for each frequency, pressure, and temperature desired. A test sample is then attached to the reflector and the procedure repeated. This method utilizes a comparison of the amplitude and phase obtained with a sample in place and a standard run with no sample.

Samples tested were 5-cm-diam discs die-cut from 0.3175-cm-thick dry material and from the same sheets used in the gravimetric analysis after soaking for one year in castor oil at 75°C. Dry samples were attached to the stainless steel reflector with Vulcalock, a rubber adhesive. Castor-oil-soaked samples could not be attached with an adhesive so instead were held in place by stretching Parafilm® (American Can Co.) over the face of the sample and onto the edge of the reflector. Preliminary tests showed no detectable change in the test results due to its presence.

The materials were tested at frequencies from 3 to 10 kHz at 1-kHz intervals and pressures of 0, 0.5, 1, 2, 4, 8, and 16 MPa (gage pressures).

G19 Hydrophone Calibrator

The USRD standard G19 hydrophone calibrator is a device used to calibrate small hydrophones by comparing the voltage response of the unknown hydrophone with that of a standard hydrophone. The G19 was used in this work primarily to compare the changes that occurred in the voltage responses of a PZT-4 element due to the use of different pressure-release materials shielding the element edge.

The basic configuration used as the test hydrophone is that shown in Fig. 5. The various pressure-release materials shielded the PZT-4 element radially and were held in place by an aluminum split-ring and collar. The G19 calibrator was filled with Fluorinert FC-75, a liquid dielectric, to approximately 1 cm from the top.

The test hydrophone was lowered into the calibrator by a nylon tire cord tied to one end to a ring stand and cemented on the other end to the aluminum collar. This configuration afforded precise positioning of the hydrophone element for the series of calibrator tests. The only parameters that were varied throughout the test series were the type of pressure-release material and the projector's frequency, which was varied from 100 to 1000 Hz in increments of 100 Hz.

A number of configurations and materials were used to shield the PZT-4 element. In some cases, rings were die cut from the various materials (both dry and castor-oil saturated) and stacked around the element, as illustrated in Fig. 6. In this way, oil soaking could be simulated by replacing dry rings with oil-soaked rings. In other cases, thin layers of material were wrapped radially around the element, as shown in Fig. 7, thus simulating oil soaking from the radial direction.

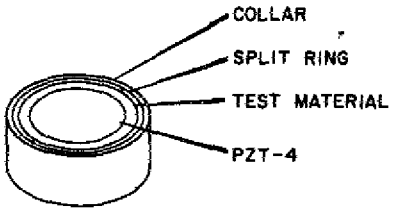

Fig. 5 — Basic configuration of test hydrophone

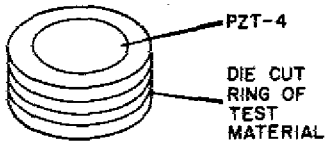

Fig. 6 — Die cut rings of cork-rubber material stacked around ceramic element

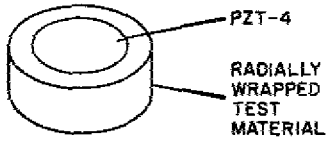

Fig. 7 — Cork-rubber material wrapped radially around ceramic element

RESULTS AND DATA REDUCTION

Microscopic Analysis

The original intent of the microscopic analysis (that is, as a visual aid in understanding the transducer fill-fluid permeation problem) was accomplished. In general, the oil-soaking process appeared as follows: The area soaked in oil was obvious from the darkening of the matrix. The fluid was diffused across a 0.5- to 2-mm region, depending on the combination of materials. The cork granules near the fluid front seemed to be either saturated or dry, with few examples in between.

None of the dyes dissolved very extensively in the castor oil; at best they produced only slight tints. In every case, however, even the slight tints could be detected in the first layer of cork; that is, the layer of cork granules with part of their surface directly exposed to the castor-oil-dye mixture. But no dye could be visually detected in any cork granule that had a layer of rubber between it and the dyed castor oil, even though castor oil was evident.

Gravimetric Analysis

Results of the gravimetric analysis are presented in the graphs designated as Figs. 8(a) through 19(a). In these graphs the ordinate is given as the flux of transducer fill fluid through the exposed surface area in mg/cm^2 (this quantity is actually the integrated flux or cumulative flow of transducer fill fluid but for brevity will be referred to as the flux), and the abscissa is given as the time in hours. Both are logarithmic scales.

Temperature dependence of fluid penetration into a composite material is complex, involving several steps with different energies of activation. It is obvious from looking at these graphs that the reaction is accelerated by an increase in temperature. It can also be seen that the slope of the

log-log plot from 100 hours (long enough to eliminate the effects of viscous flow through the exposed cork granules) to approximately 1000 hours (before the fluid fronts converge in the center and before blistering, hardening, and/or disintegration occur) is very close to 0.5. A slope of one half in the midregion, according to Fick's second law, defines a diffusion-controlled process (Appendix B). A line with a slope of one half was fitted to the data in the midregion of Figs. 8(a) through 19(a). From this k_0 was determined by extrapolating back to 1 h (at $t = 1$, $\log k = \log k_0$). Figures 8(b) through 19(b) show the relation between the extrapolated value of k_0 and the reciprocal of the absolute temperature. Relating this information to the Arrhenius Equation:

$$k_0 = \zeta \exp(-Q/R\theta) \tag{13}$$

where ζ = statistical factor,
Q = energy of activation,
θ = absolute temperature (°K),
R = gas law constant (8.314 J/mol-°K),

or

$$\ln k_0 = (-Q/R)(1/\theta) + \ln \zeta \, . \tag{14}$$

Therefore, the slope of the $\ln k_0$ vs $1/\theta$ line equals $-Q/R$.

The changes in the volume of the cork-rubber composites are given in Tables 4(a) through 14(a). This information is somewhat limited because it was not a part of the original test plan but was added after changes in the volume of the test samples became apparent. The values were found by measuring the length, width, and thickness of the samples to calculate the volume and then comparing this value to the original volume.

The shore hardness data are presented in Tables 4(b) through 14(b). Again, this was not originally planned as a test but was included after noting major changes in hardness in some samples. The values given are averages of 10 Durometer readings at the given time interval and temperature.

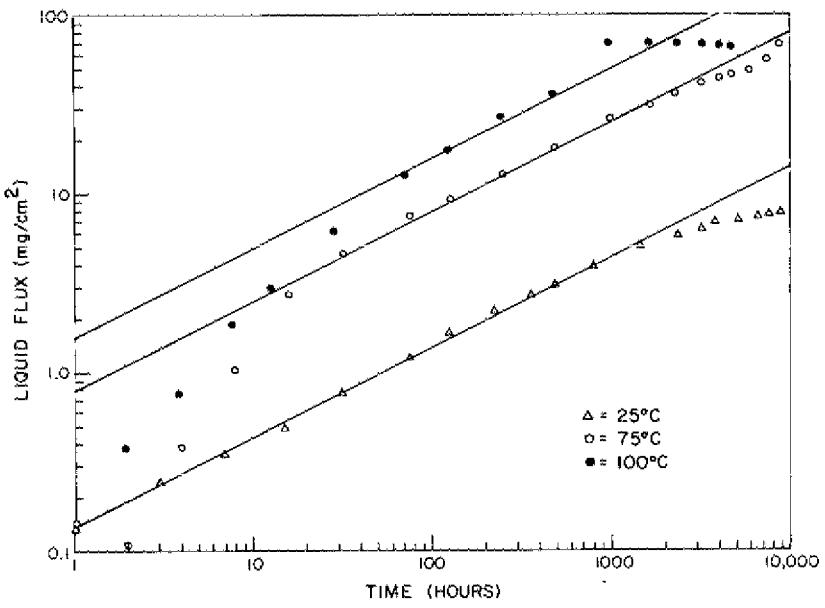

Fig. 8(a) — Gravimetric analysis of DC-100 exposed to castor oil

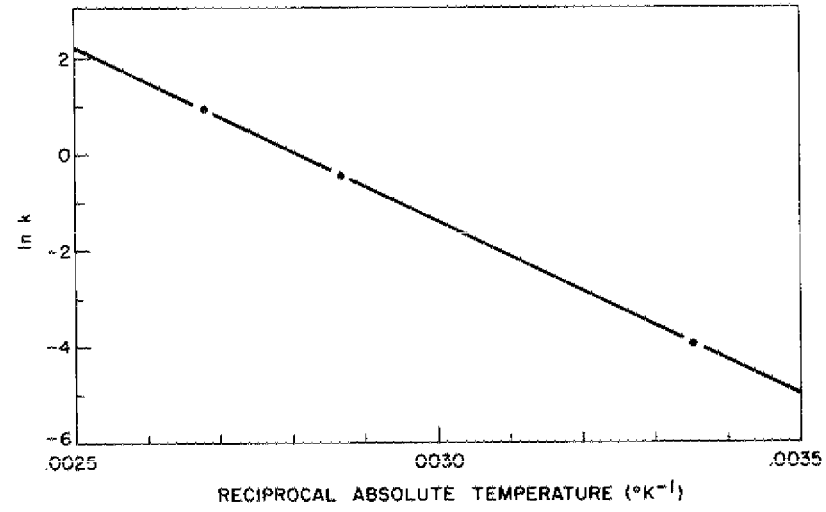

Fig. 8(b) — Arrhenius plot for DC-100 exposed to castor oil

Table 4 — Polychloroprene-Cork DC-100 Exposed to Castor Oil

(a) Changes in Volume

Elapsed Time (h)	25°C	75°C	100°C
4677			+7%
5189	0%		
6028		+2%	
7920	0%		
8760	-2%	+4%	

(b) Shore Hardness

Elapsed Time (h)	25°C	75°C	100°C
0	68	68	68
4677			22
5189	63		
6028		57	
7920	67		
8760	64	54	

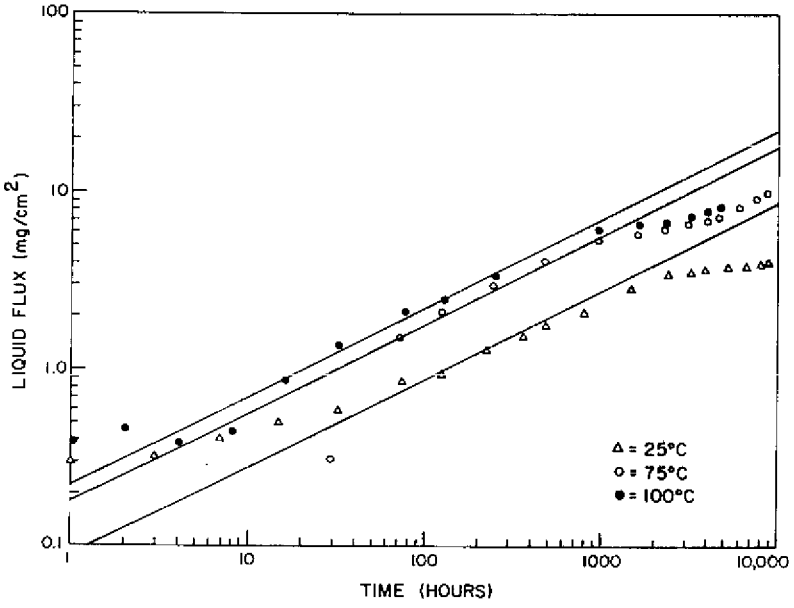

Fig. 9(a) — Gravimetric analysis of DC-100 exposed to silicone oil

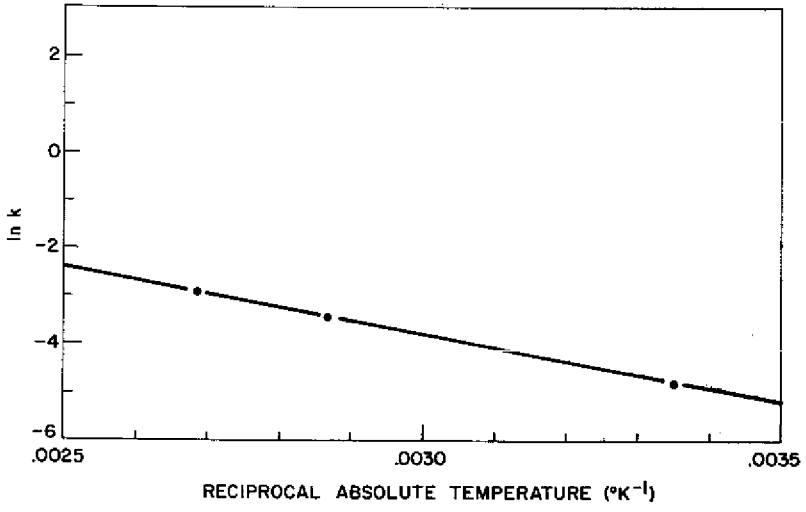

Fig. 9(b) — Arrhenius plot for DC-100 exposed to silicone oil

Table 5 — Polychloroprene-Cork DC-100 Exposed to Silicone Oil

(a) Changes in Volume

Elapsed Time (h)	25°C	75°C	100°C
4677			-6%
5189	-1%		
6028		-3%	
7920	-2%		
8760	-3%	-4%	

(b) Shore Hardness

Elapsed Time (h)	25°C	75°C	100°C
0	68	68	68
4677			95
5189	64		
6028		90	
7920	68		
8760	65	101	

Table 6 — Polychloroprene-Cork DC-100 Exposed to PAG

(a) Changes in Volume

Elapsed Time (h)	25°C	75°C	100°C
4677	+3%		+6%
5189		+4%	
6028	+2%		
7920	+5%	+3%	
8760			

(b) Shore Hardness

Elapsed Time (h)	25°C	75°C	100°C
0	68	68	68
4677	57	73	52
5189			
6028	61	78	
7920	60		
8760			

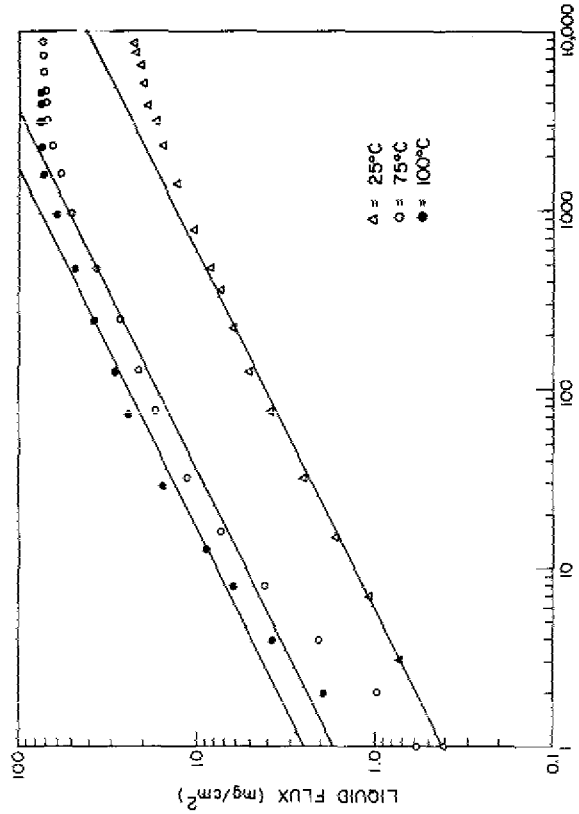

Fig. 10(a) — Gravimetric analysis of DC-100 exposed to PAG

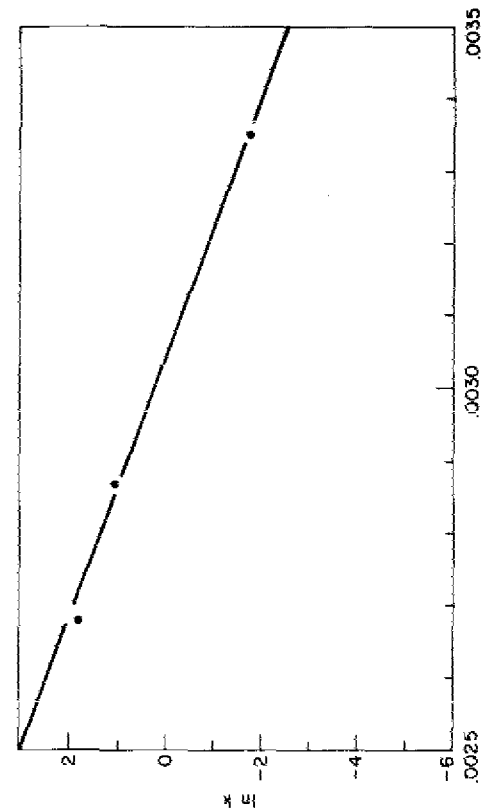

Fig. 10(b) — Arrhenius plot for DC-100 exposed to PAG

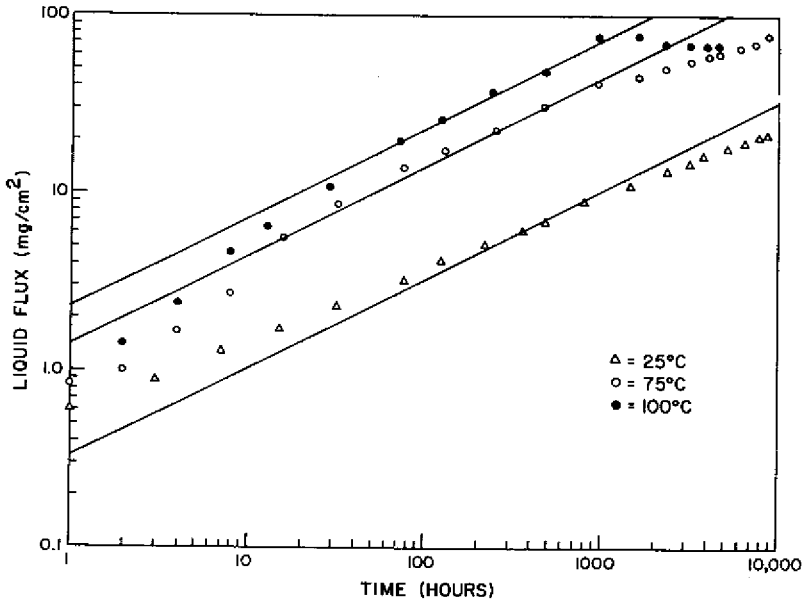

Fig. 11(a) — Gravimetric analysis of DC-116 exposed to castor oil

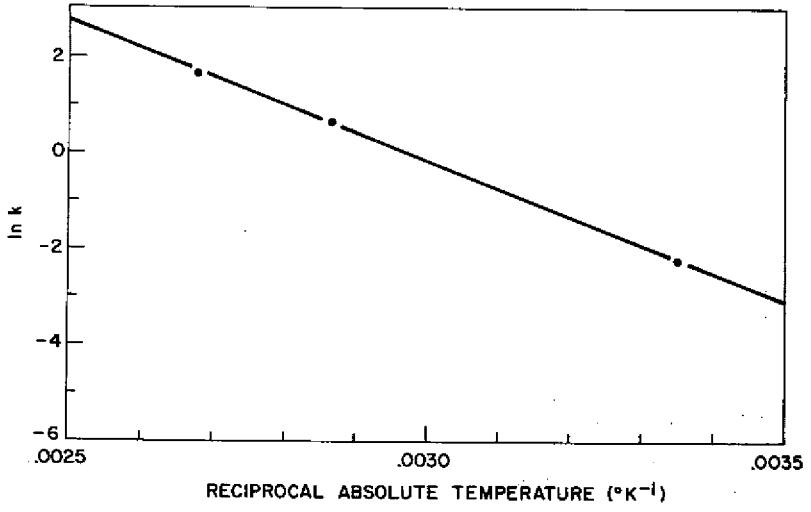

Fig. 11(b) — Arrhenius plot for DC-116 exposed to castor oil

Table 7 — Polychloroprene-Cork DC-116 Exposed to Castor Oil

(a) Changes in Volume

Elapsed Time (h)	25°C	75°C	100°C
4677			+5%
5189	0%		
6028		+3%	
7920	0%		
8760	-2%	+5%	

(b) Shore Hardness

Elapsed Time (h)	25°C	75°C	100°C
0	70	70	70
4677			21
5189	61		
6028		59	
7920	67		
8760	65	56	

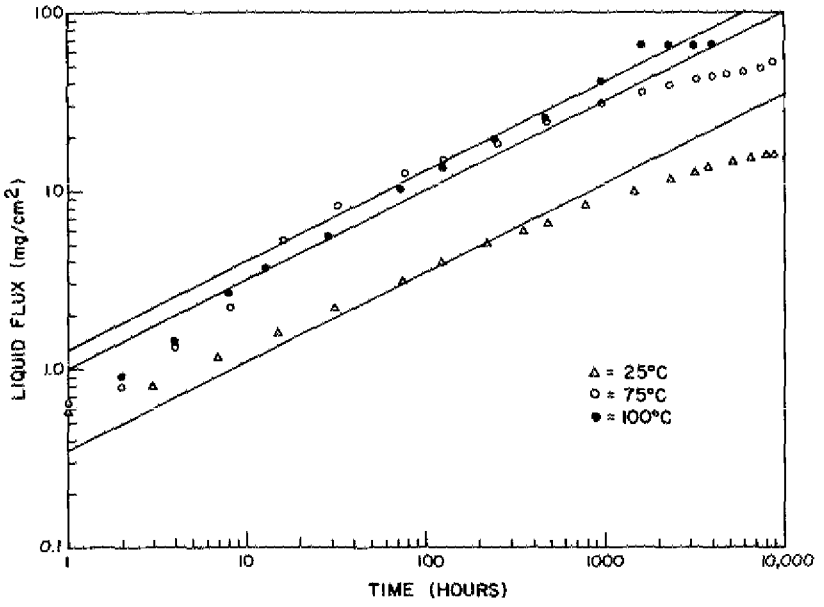

Fig. 12(a) — Gravimetric analysis of NC-710 exposed to castor oil

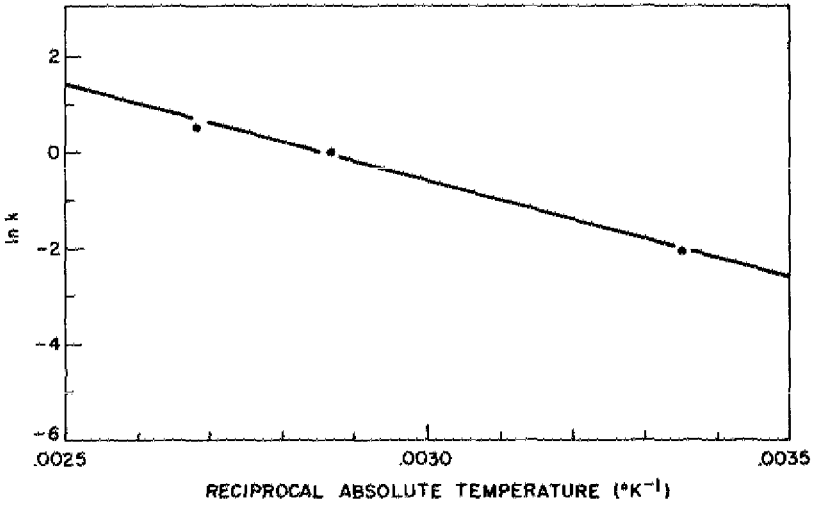

Fig. 12(b) — Arrhenius plot for NC-710 exposed to castor oil

Table 8 — Polynitrilebutadiene-Cork NC-710 Exposed to Castor Oil

(a) Changes in Volume

Elapsed Time (h)	25°C	75°C	100°C
4677			+4%
5189	0%		
6028		0%	
7920	0%		
8760	-3%	0%	

(b) Shore Hardness

Elapsed Time (h)	25°C	75°C	100°C
0	73	73	73
4677			43
5189	66		
6028		69	
7920	71		
8760	69	69	

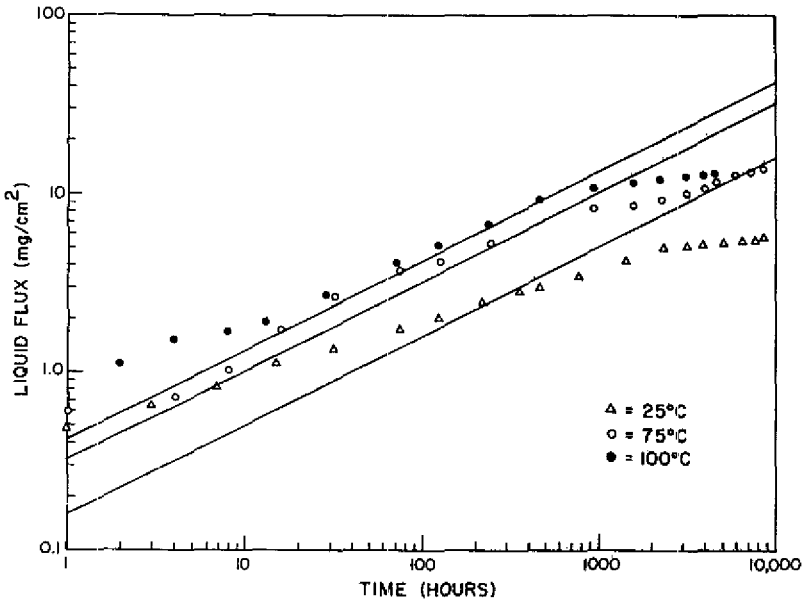

Fig. 13(a) — Gravimetric analysis of NC-710 exposed to silicone oil

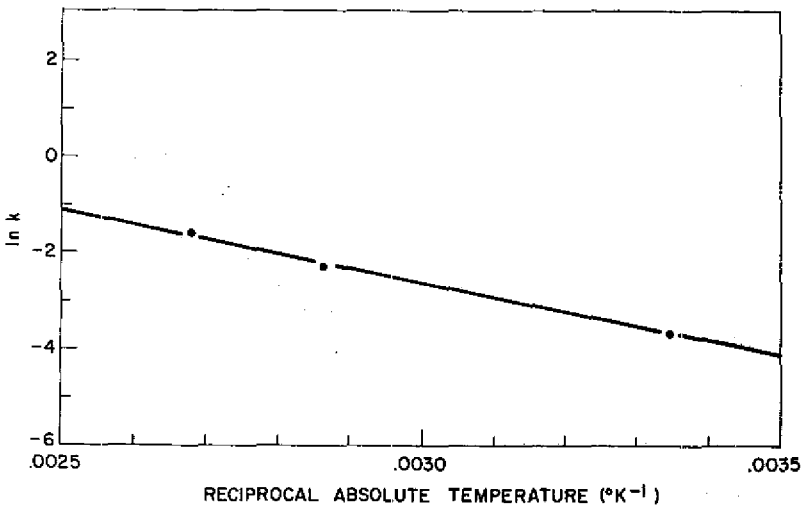

Fig. 13(b) — Arrhenius plot for NC-710 exposed to silicone oil

Table 9 — Polynitrilebutadiene-Cork NC-710 Exposed to Silicone Oil

(a) Changes in Volume

Elapsed Time (h)	25°C	75°C	100°C
4677			-5%
5189	0%		
6028		-3%	
7920	-1%		
8760	-3%	-4%	

(b) Shore Hardness

Elapsed Time (h)	25°C	75°C	100°C
0	73	73	73
4677			96
5189	68		
6028		96	
7920	72		
8760	69	100	

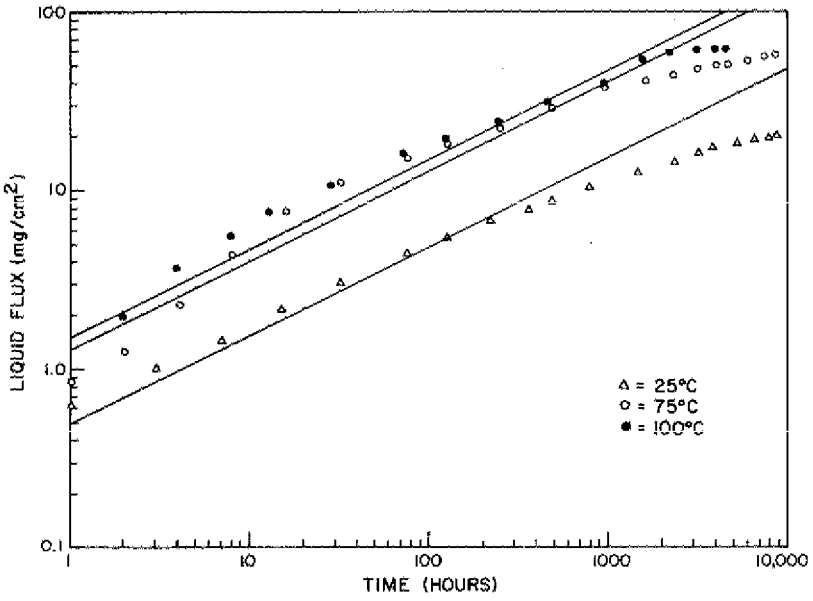

Fig. 14(a) — Gravimetric analysis of NC-710 exposed to PAG

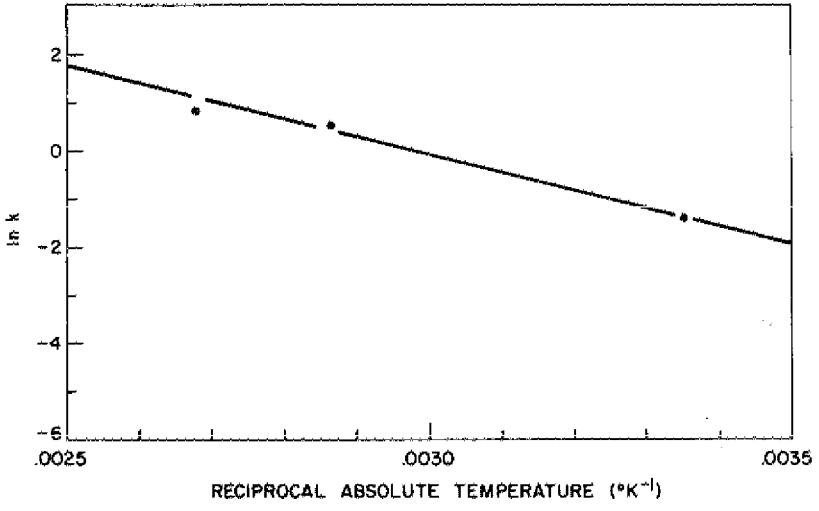

Fig. 14(b) — Arrhenius plot for NC-710 exposed to PAG

Table 10 — Polynitrilebutadiene-Cork NC-710 Exposed to PAG

(a) Changes in Volume

Elapsed Time (h)	25°C	75°C	100°C
4677			+3%
5189	+1%		
6028		+1%	
7920	0%		
8760	+1%	0%	

(b) Shore Hardness

Elapsed Time (h)	25°C	75°C	100°C
0	73	73	73
4677			66
5189	64		
6028		79	
7920	69		
8760	65	88	

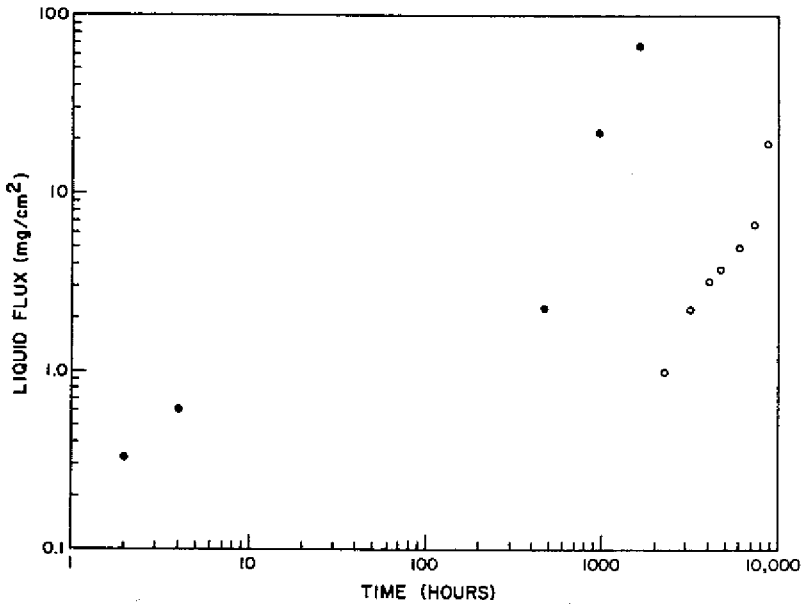

Fig. 15 — Gravimetric analysis of NC-775 exposed to castor oil

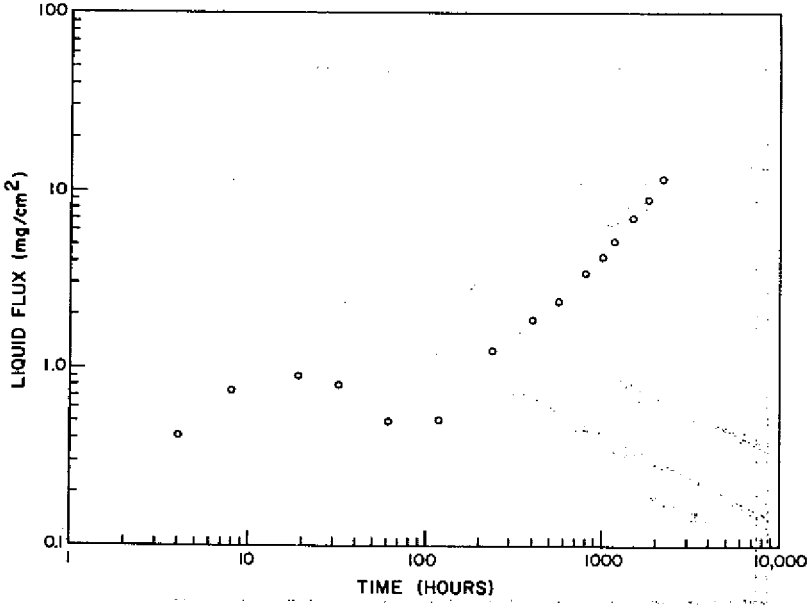

Fig. 16 — Gravimetric analysis of NC-775 exposed to PAG

Table 11 — Polynitrilebutadiene NC-775 Exposed to Castor Oil

(a) Changes in Volume

Elapsed Time (h)	25°C	75°C	100°C
4677			
5189	0%		
6028		-2%	
7920	0%		
8760	-4%	0%	

(b) Shore Hardness

Elapsed Time (h)	25°C	75°C	100°C
0	78	78	78
4677			
5189	65		
6028		75	
7920	70		
8760	74	72	

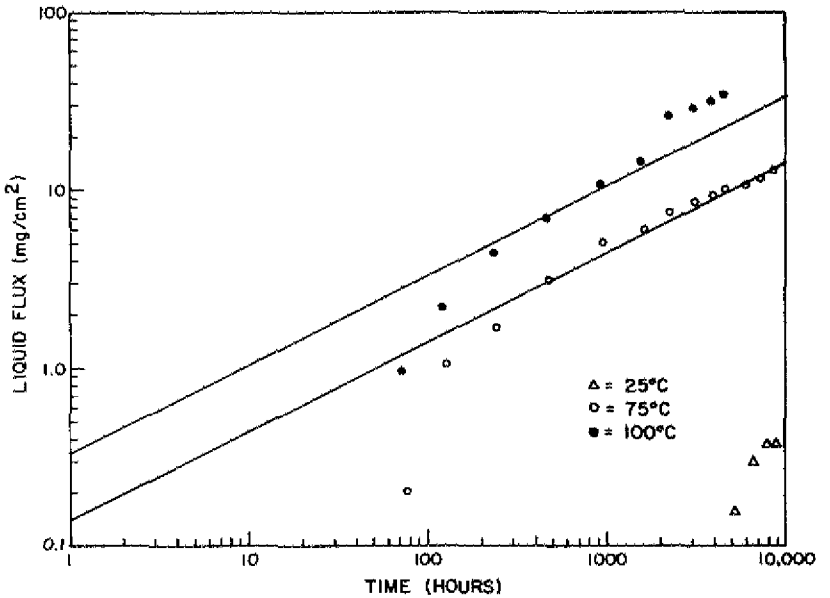

Fig. 17(a) — Gravimetric analysis of LC-800 exposed to castor oil

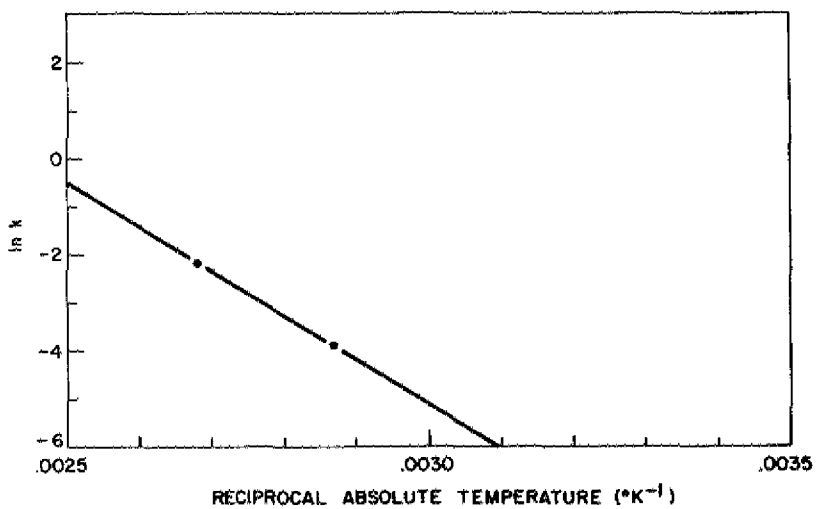

Fig. 17(b) — Arrhenius plot for LC-800 exposed to castor oil

Table 12 — Silicone Rubber-Cork LC-800 Exposed to Castor Oil

(a) Changes in Volume

Elapsed Time (h)	25°C	75°C	100°C
4677			+3%
5189	0%		
6028		0%	
7920	0%		
8760	-2%	-2%	

(b) Shore Hardness

Elapsed Time (h)	25°C	75°C	100°C
0	72	72	72
4677			58
5189	65		
6028		64	
7920	70		
8760	68	70	

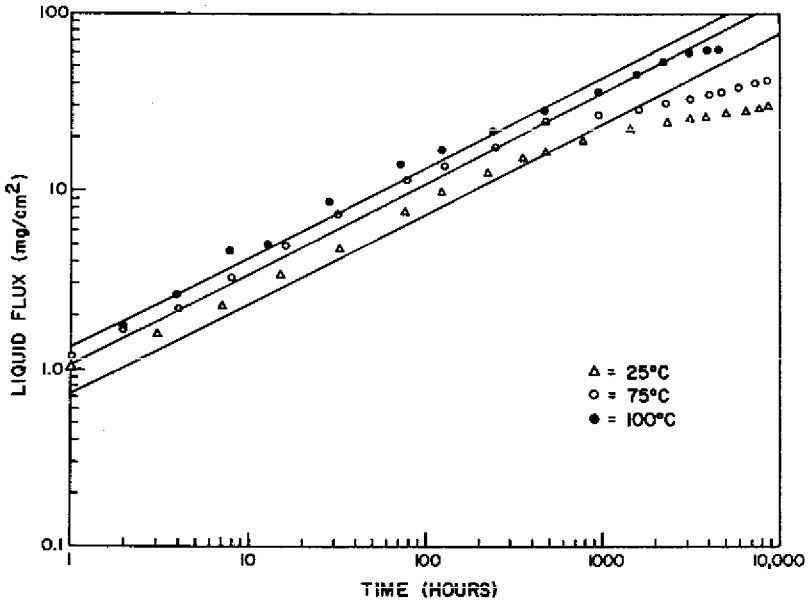

Fig. 18(a) — Gravimetric analysis of LC-800 exposed to silicone oil

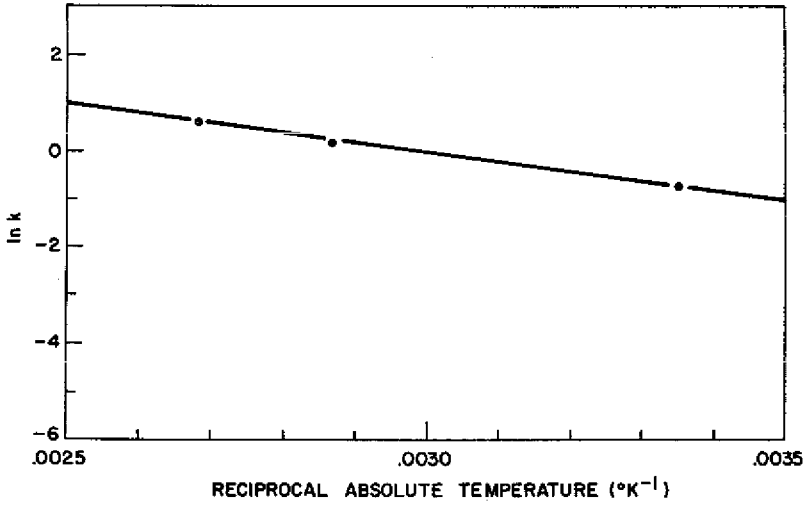

Fig. 18(b) — Arrhenius plot for LC-800 exposed to silicone oil

Table 13 — Silicone Rubber-Cork LC-800 Exposed to Silicone Oil

(a) Changes in Volume

Elapsed Time (h)	25°C	75°C	100°C
4677			+11%
5189	+8%		
6028		+11%	
7920	+8%		
8760	+8%	+9%	

(b) Shore Hardness

Elapsed Time (h)	25°C	75°C	100°C
0	72	72	72
4677			61
5189	55		
6028		54	
7920	60		
8760	57	60	

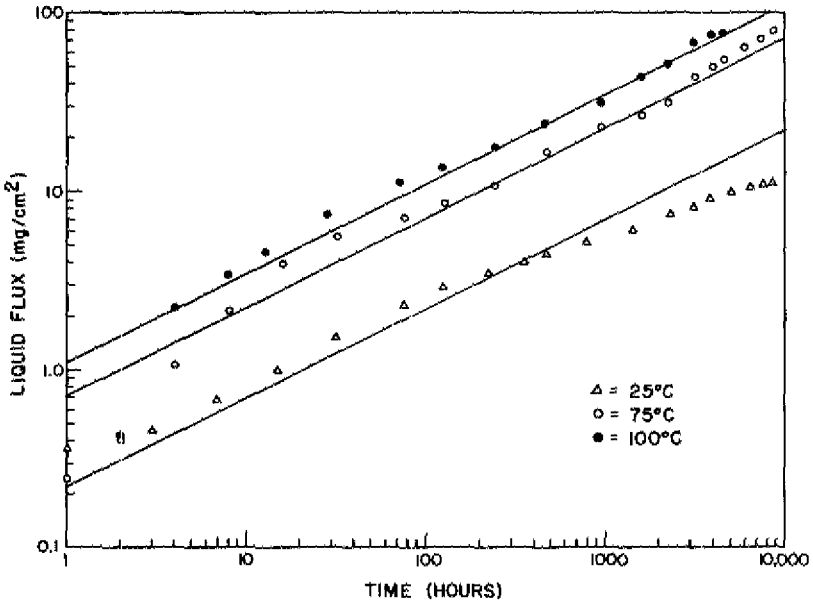

Fig. 19(a) — Gravimetric analysis of LC-800 exposed to PAG

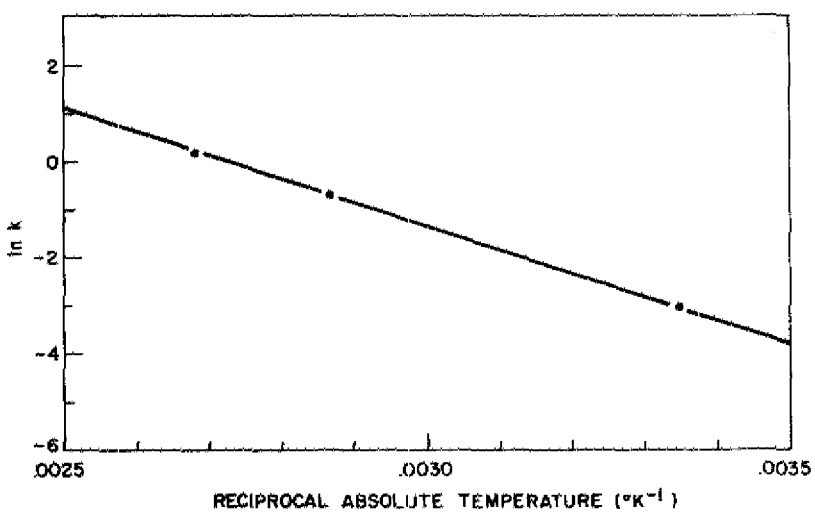

Fig. 19(b) — Arrhenius plot for LC-800 exposed to PAG

Table 14 — *Silicone Rubber-Cork LC-800* Exposed to PAG

(a) Changes in Volume

Elapsed Time (h)	25°C	75°C	100°C
4677			+10%
5189	+2%		
6028		+9%	
7920	+2%		
8760	+2%	+10%	

(b) Shore Hardness

Elapsed Time (h)	25°C	75°C	100°C
0	72	72	72
4677			40
5189	58		
6028		49	
7920	62		
8760	59	52	

Microtome Sectioning

The results of the microtome sectioning and weighing tests are shown in Figs. 20 through 23, where the density (g/cm^3) of the cork-rubber composite and castor-oil diffusion pair are plotted against the depth of penetration (mm). The lower dashed line is the density of the material before being exposed to castor oil, and the upper dashed line is the maximum density of the material after complete castor-oil saturation. Each graph contains data for six months (Δ), nine months (○), and twelve months (●) at 75°C in castor oil. Samples were sectioned after three months, but the data were not usable because the penetration was less than the thickness of the section. For the same reason 25°C sectioning data were not useful. The data points shown were found by taking a running weighted average of the density from two separate samples at the designated time interval and temperature.

Acoustic Impedance Tube

Results obtained from the acoustic impedance tube are represented in Figs. 24 through 28. Each graph shows the sound speed (m/s) for the dry composite (lower solid curve) and the sound speed of the same composite after one year in castor oil at 75°C (upper solid curve) as a function of pressure (MPa). On the same graphs the attenuation (dB/m of material) is represented by dashed lines. The upper dashed line is the attenuation of sound in the unsoaked composite, whereas the lower dashed line represents the attenuation data from castor-oil-soaked material as a function of pressure. Data reduction done by the FORTRAN program are given in Appendix C. The equation relating the input impedance of the test sample to the propagation constant is transcendental and cannot be solved explicitly for attenuation (α) and sound speed (c). For this reason the values for α and c are obtained from a FORTRAN program that converges on the solution by making successive approximations. The input consists of pressure, frequency, sample length, sample density, amplitude of standard, amplitude with sample, phase angle of standard, and phase angle with sample. The output is in the form of sound speed, attenuation, phase shift, and reflection coefficient.

G19 Hydrophone Calibrator

The results of tests in the G19 calibrator are shown in Figs. 29 through 34. Figure 29 shows the relation between the voltage sensitivity of an unshielded PZT-4 ceramic element (lower curve), the F61 standard hydrophone (straight line at −207 dB), and PZT-4 element shielded by dry DC-100 (upper curve). The relative voltage sensitivities of a PZT-4 element radially wrapped with dry material and with castor-oil-soaked material are illustrated in Figs. 30 through 34. In each graph the upper curve is for the element wrapped with dry material and the lower curve is for the element wrapped with composite, which was soaked in castor oil at 75°C for one year.

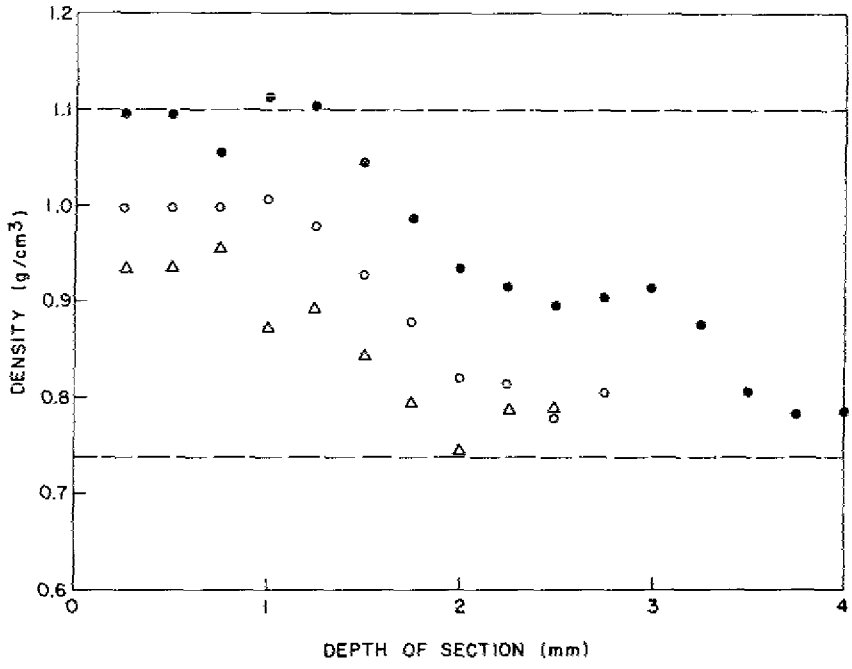

Fig. 20 — Microtome sectioning analysis of DC-100 exposed to castor oil at 75°C

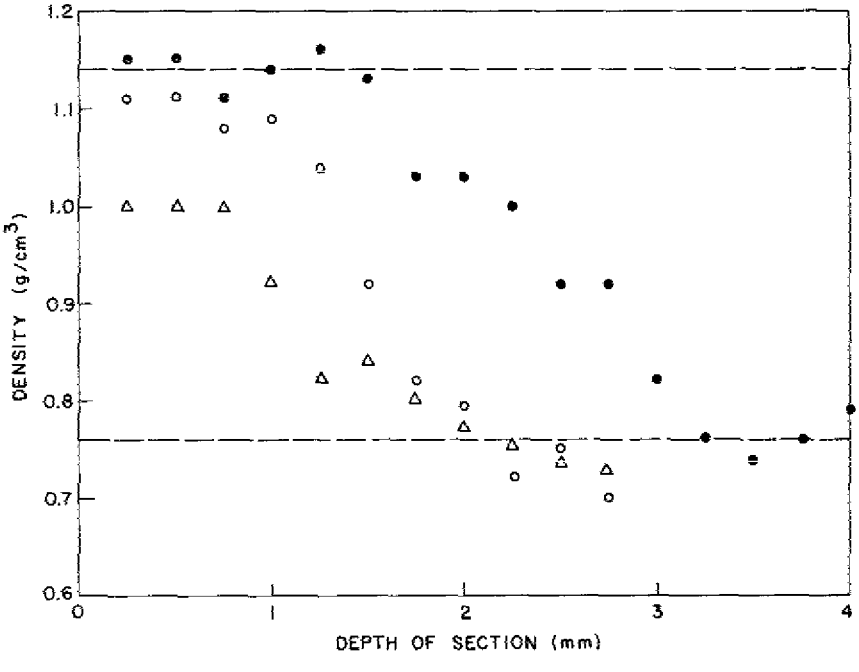

Fig. 21 — Microtome sectioning analysis of DC-116 exposed to castor oil at 75°C

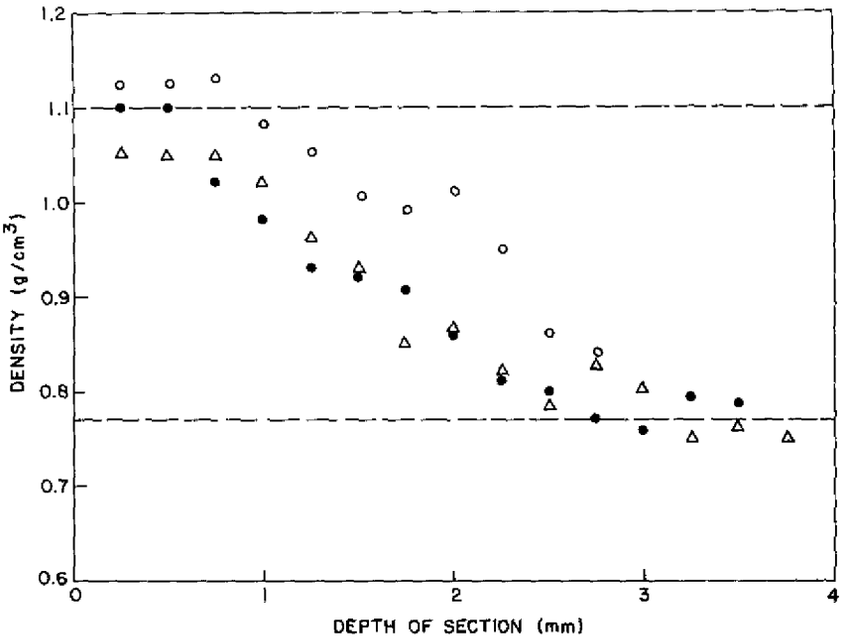

Fig. 22 — Microtome sectioning analysis of NC-710 exposed to castor oil at 75°C

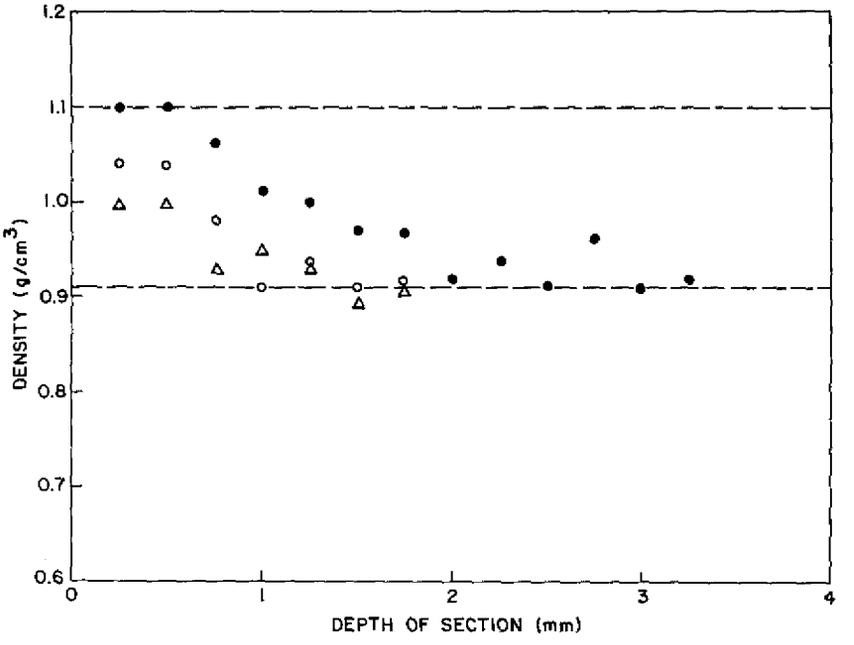

Fig. 23 — Microtome sectioning analysis of NC-775 exposed to castor oil at 75°C

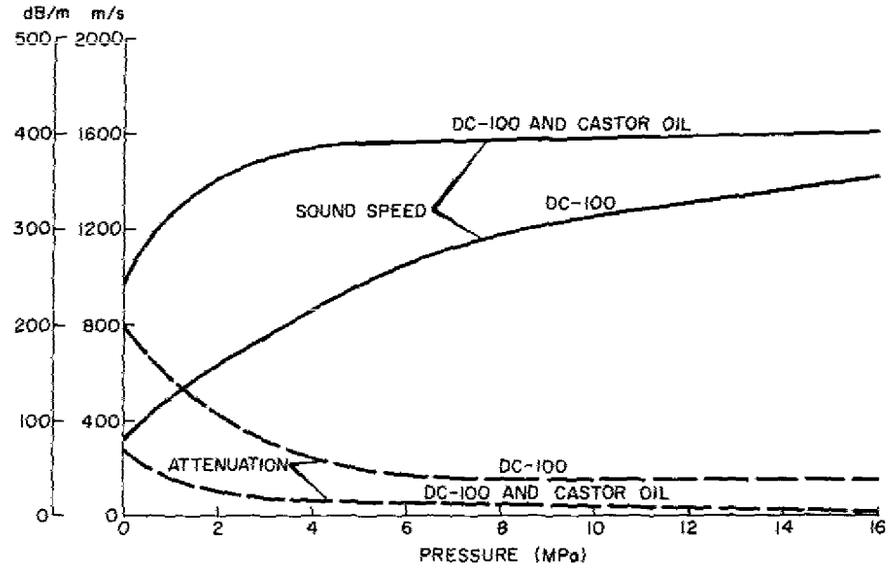

Fig. 24 — Acoustic impedance-tube test results for dry and castor-oil-soaked DC-100

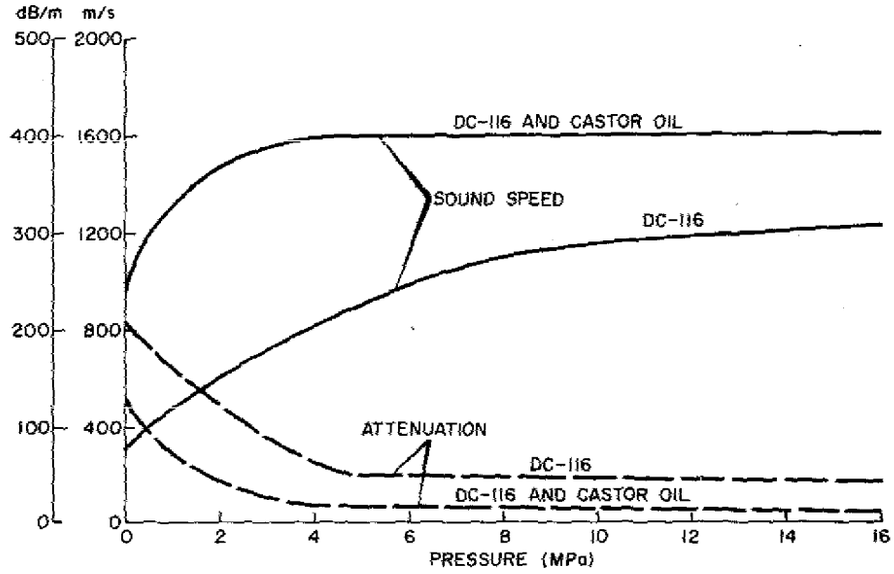

Fig. 25 — Acoustic impedance-tube test results for dry and castor-oil-soaked DC-116

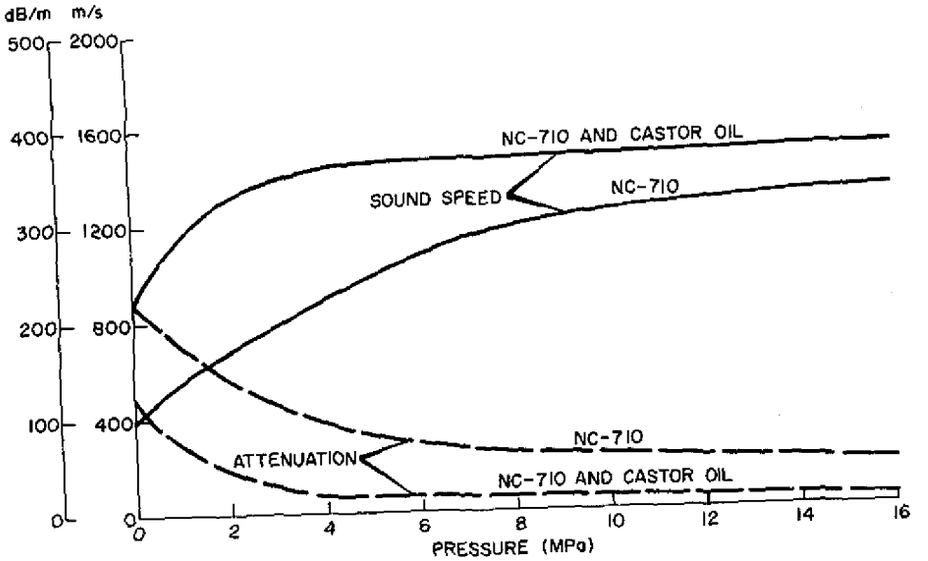

Fig. 26 — Acoustic impedance-tube test results for dry and castor-oil-soaked NC-710

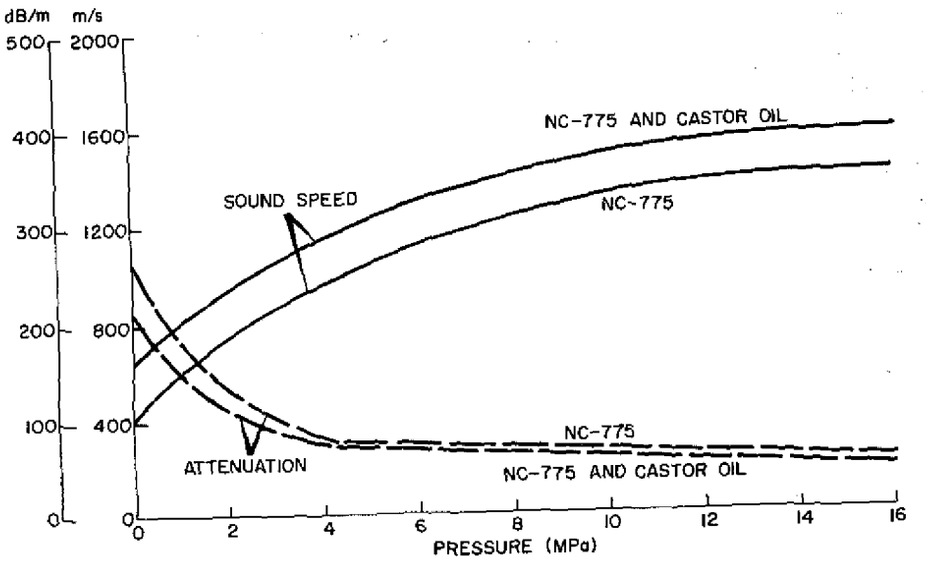

Fig. 27 — Acoustic impedance-tube test results for dry and castor-oil-soaked NC-775

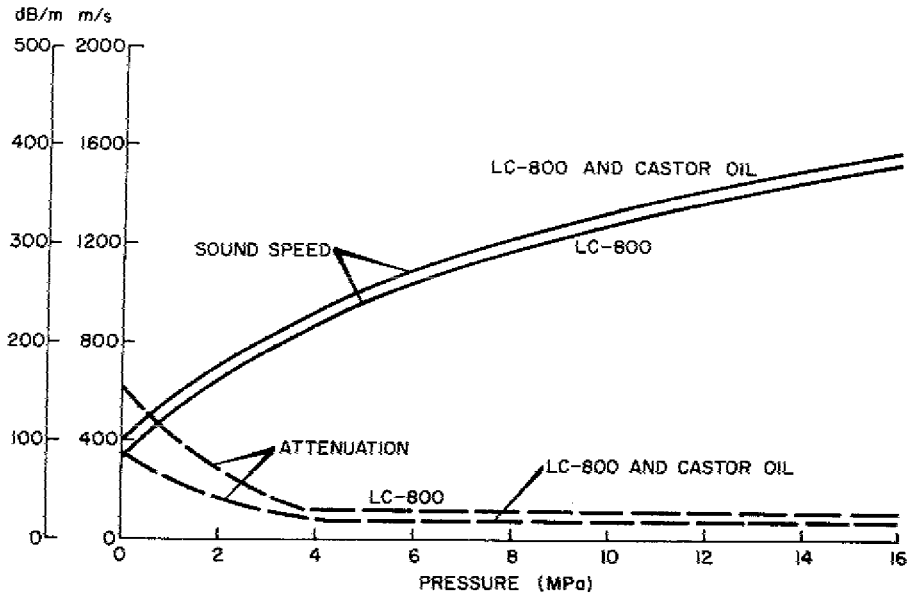

Fig. 28 — Acoustic impedance-tube test results for dry and castor-oil-soaked LC-800

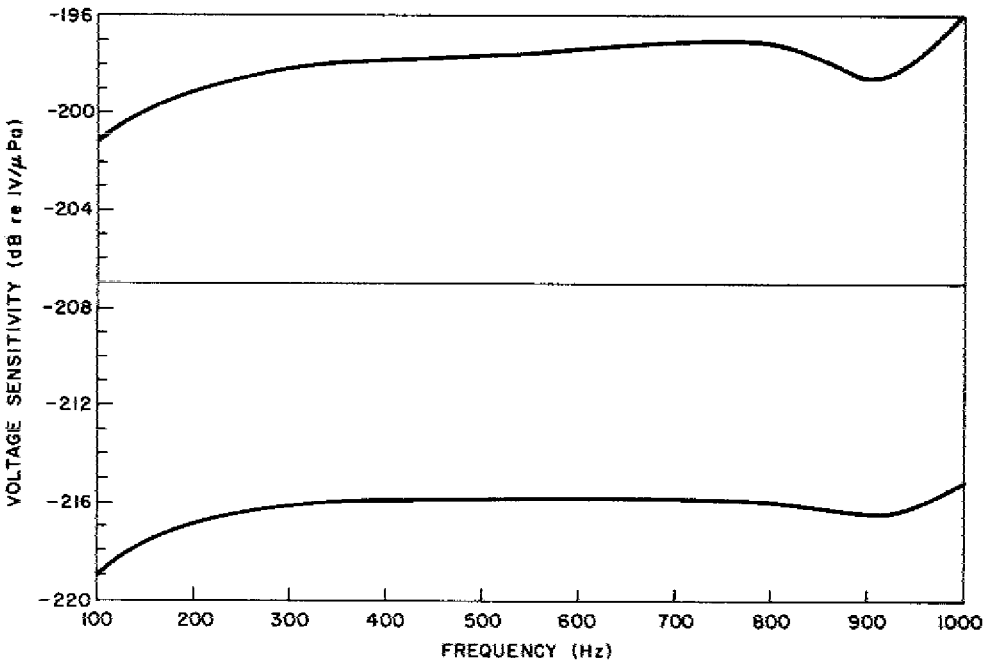

Fig. 29 — Comparison of the voltage sensitivity of an unshielded PZT-4 disc (lower curve) to an F61 standard hydrophone (middle line) and to a DC-100 radially shielded PZT-4 disc (upper curve)

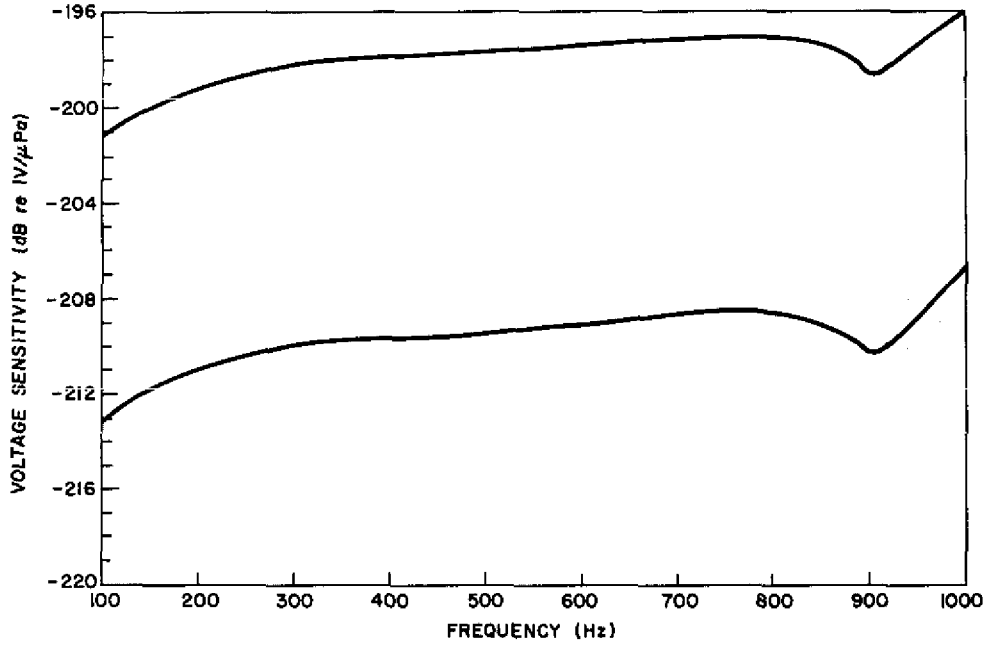

Fig. 30 — Voltage sensitivity of a PZT-4 disc radially shielded with dry DC-100 (upper curve) and with castor-oil-soaked DC-100 (lower curve)

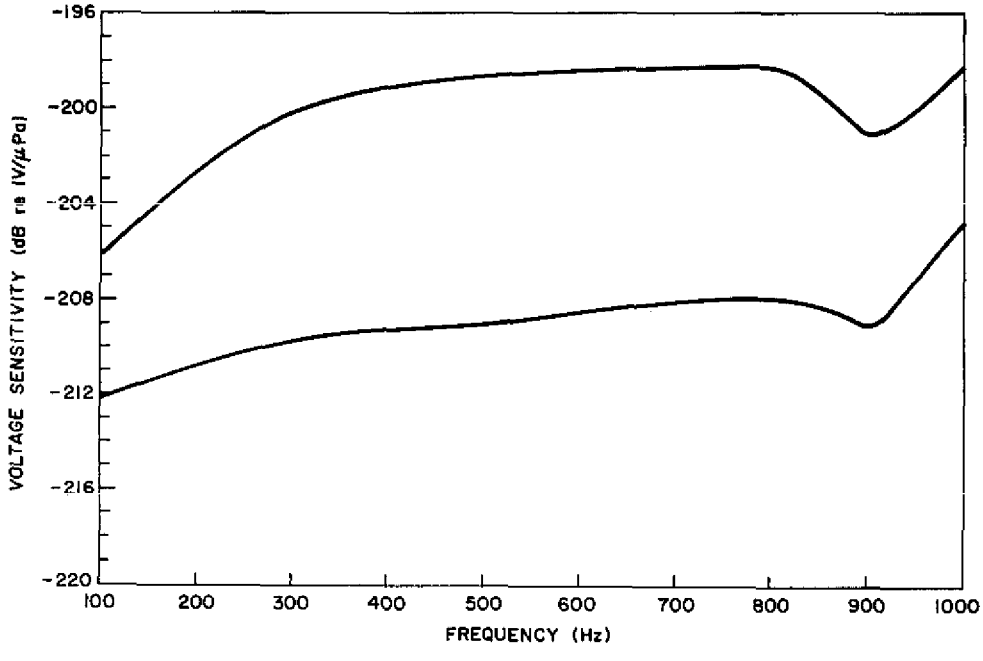

Fig. 31 — Voltage sensitivity of a PZT-4 disc radially shielded with dry DC-116 (upper curve) and with castor-oil-soaked DC-116 (lower curve)

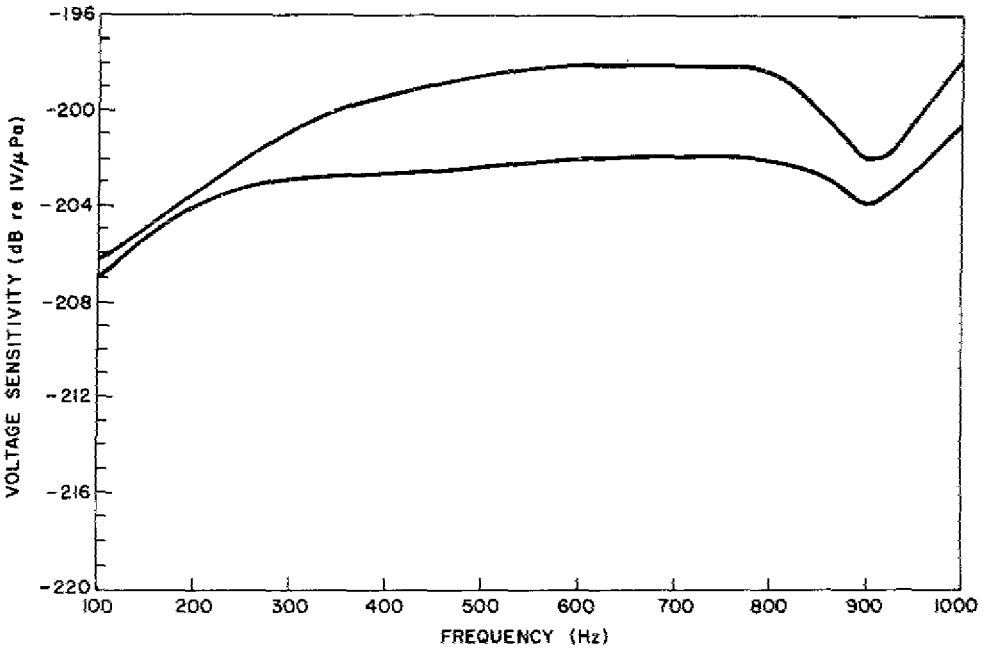

Fig. 32 — Voltage sensitivity of a PZT-4 disc radially shielded with dry NC-710 (upper curve) and with castor-oil-soaked NC-710 (lower curve)

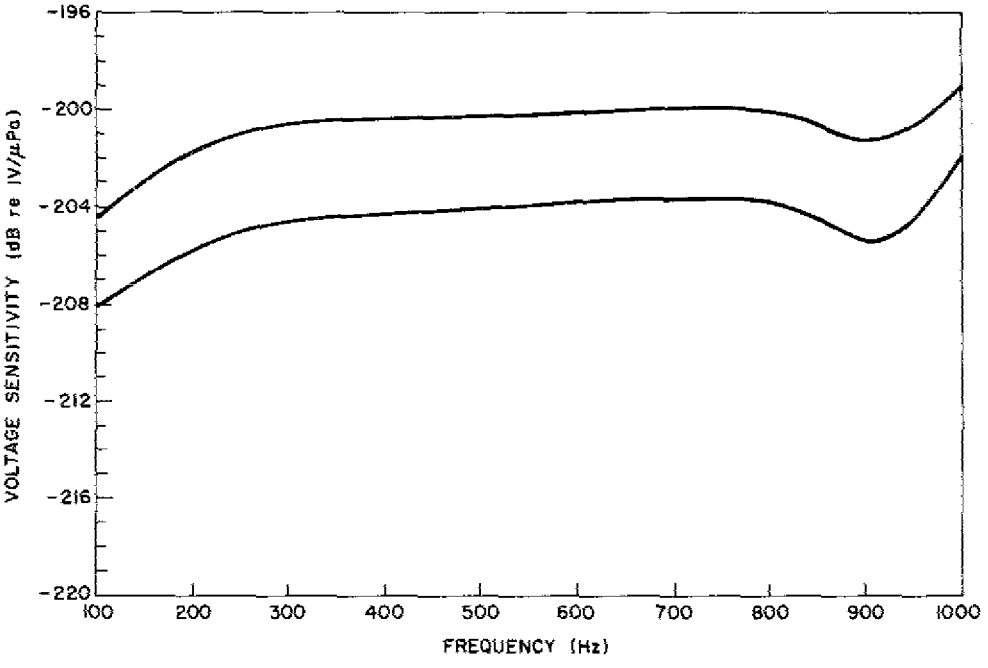

Fig. 33 — Voltage sensitivity of a PZT-4 disc radially shielded with dry NC-775 (upper curve) and with castor-oil-soaked NC-775 (lower curve)

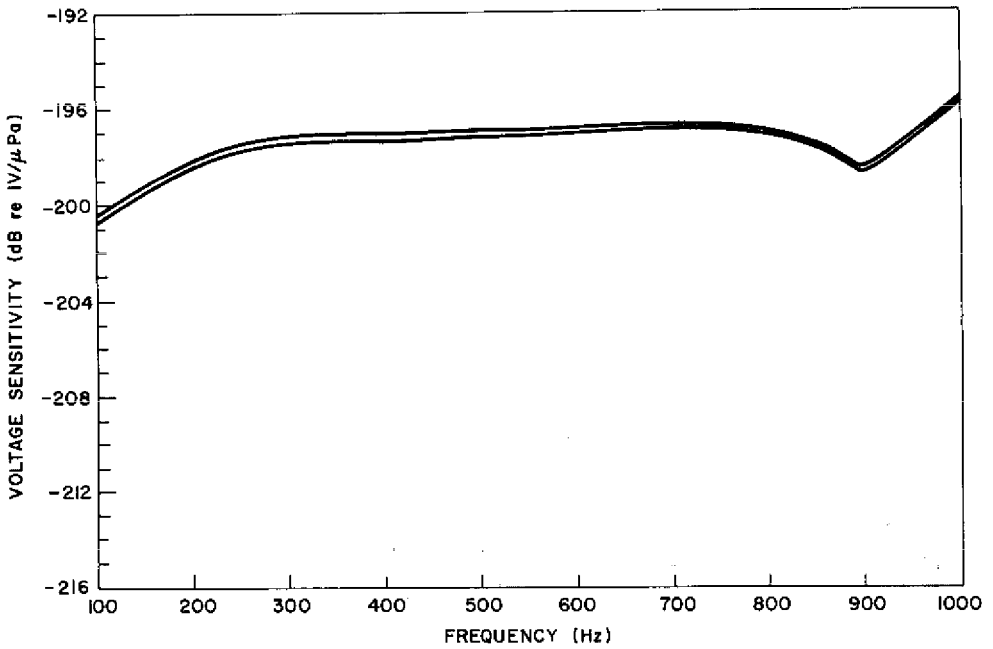

Fig. 34 — Voltage sensitivity of a PZT-4 disc radially shielded with dry LC-800 (upper curve) and with castor-oil-soaked LC-800 (lower curve)

DISCUSSION OF RESULTS

Microscopic Analysis

Results of the microscopic analysis point toward a three-part castor-oil permeation mechanism in cork-rubber composites. The first part is a viscous flow of castor oil through the porous cork granules that compose the outer surface. These exposed granules appear saturated with oil soon after exposure to castor oil and are tinted by the castor-oil-dye mixture. Secondly, the movement of the castor oil through the rubber matrix is by diffusion. This is supported by observing that the castor oil moves very slowly thorugh the rubber and that the first layer of rubber encountered by the castor-oil-dye mixture effectively filters out any dye molecules present. A third part of the permeation is a combination of the aforementioned mechanisms. That is, although the castor oil flows through the inner cork granules, it is limited by the amount of castor oil available due to the slow rate of diffusion through the rubber matrix. Each of the individual inner cork granules appears uniformly soaked with castor oil but less saturated with distance from the exposed surface.

Gravimetric Analysis

Results of the gravimetric analysis support and quantitate the intuitive findings of the microscopic investigation. In most instances the liquid flux through the exposed surface is at a much faster rate in the first few hours than at any other time. This supports the theory of oil flowing into the exposed cork granules. The only exception to this rapid increase in weight was found in the NC-775, a low-cork-content composite, which was found to disintegrate rapidly (especially at elevated temperatures). Thus, the weight gain of the relatively few cork granules was more than offset by the weight loss of the disintegrating nitrile rubber. This may also explain why the NC-710 composite has a relatively low rate of weight gain in the first few hours when compared to the other

composites. Having a higher cork content than the NC-775 composite, it can gain more weight from the surface exposure, while at the same time the lower percent nitrile rubber will lose less weight through degradation. The net effect is an apparent low-liquid flux in the first few hours.

In the second phase of liquid penetration (that is, diffusion into the rubber matrix), the slope of most of the graphs approximates 0.5. The lines drawn to represent the slope on the (a) versions of Figs. 8 through 19 were all purposely drawn at a slope of one half to illustrate how closely each composite-liquid pair actually comes to a diffusion-controlled process. Again, the only material to deviate significantly from the slope of 0.5 to the 100- to 1000-h range was the type NC-775. Composite NC-710 in silicone oil at 25°C also did not follow a slope of one half, but the 75° and 100°C curves did conform.

After approximately 1000 h, again with the exception of the type NC-775, the liquid flux slowed even further. This is attributable to the convergence of the liquid front in the center of the samples as the total sample approaches saturation.

Another important result of the gravimetric analysis is the determination of the activation energies and preexponential factors of the diffusion pairs. Table 15 shows these values as determined from data in the (b) version of Figs. 8 through 19. The energies of activation for type NC-775 could not be determined with this technique. Given the energy of activation, changes in the cork-rubber composite due to liquid absorption can be determined at any temperature (that is, within limits of change-of-state of the liquid, further curing of the polymer, etc.). This can be done by solving a proportional equation such as

$$r_1/r_2 = \left[\zeta \exp\left(-Q/R\theta_1\right)\right] / \left[\zeta \exp\left(-Q/R\theta_2\right)\right] , \tag{15}$$

where r_1 is the known rate of change of a material property at a test temperature of θ_1, and r_2 is the unknown rate of change at temperature θ_2. Simplifying leaves

$$r_1/r_2 = \exp\left(-Q/R\right) \left[(1/\theta_2) - (1/\theta_1)\right] \tag{16}$$

as the equation to find the unknown rate.

An important possibility for such calculations is the likelihood that the activation energy determined gravimetrically is the same as that for other basic properties. That is, a single accelerated test can be performed for some other important property (e.g., tear strength), and the equivalent test time for any other temperature may be calculated with the activation energies from Table 15 substituted into Eq. (16).

It was evident that an acceleration temperature of 100°C is somewhat too high for some cork-rubber composites. After only 30 days in castor oil at 100°C, the type DC-116 began to disintegrate along the edges and the type NC-775 developed castor-oil-filled *blisters* over its entire surface. The silicone oil tests at 100°C showed the types DC-100 and NC-710 shrank in volume by about 5% and became very hard and brittle, while the type LC-800 swelled by about 10%.

Microtome Sectioning

The most enlightening test results were those involving the microtome sectioning of the castor-oil-soaked composites. The preceding tests pointed very strongly toward a diffusion-controlled process, usually at a highly accelerated rate for the first few hours and then slowly dropping off.

Table 15 — Preexponential Factors (ζ, in kg/m) and Activation Energies (Q, in J/mol) for Absorption of Oils by Cork-Rubber Composites

Type	Castor Oil		Silicone Oil		PAG	
	ζ	Q	ζ	Q	ζ	Q
DC-100	110	55,800	[a]	[a]	139	51,700
DC-116	17.4	40,600	[b]	[b]	[b]	[b]
NC-710	0.23	20,200	0.024	9,560	38.9	43,800
NC-775	[b]	[b]	[a]	[a]	[b]	[b]
LC-800	1330	77,200	0.16	14,800	14.7	42,600

[a] Unreliable data.
[b] Not tested.

After a few hundred hours, the liquid flux approximated that expected in a diffusion process. The microtome sectioning told how much castor oil was present at any given depth of penetration and, therefore, led to an understanding of what is different in this diffusion-controlled process.

A close examination of Fig. 20 shows a definite pattern to the decrease in density with depth of penetration of the castor oil. The set of points for each time interval follows the same pattern of a density *plateau* followed by a somewhat smooth drop in density. Also, the density *plateau* increases in height at approximately a constant rate to the fully saturated state. The width of density *plateau* seems to have a square root of time dependence. Beyond the area of constant density with depth, the drop-off in density has a shape relatively close to that of the error function, which is so prevalent in diffusion of temperature and of metals.

Idealized curves were drawn for the type DC-100 using the above-mentioned concepts. According to the gravimetric data, total saturation by castor oil produces a maximum density of 1.10 g/cm^3. The corresponding maximum depth of penetration of the density *plateau* is 1.25 mm after 1 year at 100°C. The degree of curvature of the error function was determined by solving a slightly modified version of the general diffusion equation for the diffusivity, as found in Reed-Hill [11],

$$N_A = N_{A_1} + \left(N_{A_2} - N_{A_1}\right)\left(1 - \operatorname{erf}\frac{x}{2(\tilde{D}t)^{1/2}}\right), \tag{17}$$

where N_A = fraction of oil saturation at depth of penetration x,
N_{A_1} = fraction of oil saturation far into the composite sample,
N_{A_2} = fraction of oil saturation at the composite-oil interface,
t = time in hours,
$\tilde{D}$ = diffusivity.

In all of these cases $N_{A_1} = 0$ and $N_{A_2} = 1$. The diffusivity is easily calculated by determining from experimental data both x and t for a given degree of saturation. If a value of $N_A = 0.5$ is chosen, then Eq. (17) becomes

$$0.5 = \operatorname{erf}\frac{x}{2(\tilde{D}t)^{1/2}}. \tag{18}$$

So, from error function tables

$$0.477 = \frac{x}{2(\tilde{D}t)^{1/2}} \tag{19}$$

or

$$\tilde{D} = \frac{x^2}{0.954t} \cdot \tag{20}$$

From the curve in Fig. 20 for 1 year (t = 8760 h), x = 0.7 mm (measured from the shoulder of the curve to the point of half saturation). Therefore, $\tilde{D} = 6 \times 10^{-5}$ mm^2/h. Substituting this constant value back into Eq. (17) and varying N_A yields the appropriate curve. The curve for 9 months was found by multiplying the density increase due to the castor-oil saturation by 0.75 and the depth of the density *plateau* for 1 year by $(0.75)^{1/2}$. To find the appropriate error function, D remains constant while t = 6570 (0.75 year). The 6- and 3-month curves were found in a similar manner, always keeping D constant. These idealized curves for the DC-100 composite in castor oil at 75°C are shown in Fig. 35.

The above procedure was followed to generate idealized curves for the type DC-116 (Fig. 36) with maximum density being reached in the plateau region after 10 months at 75°C and a diffusivity of 1.2×10^{-4} mm^2/h. The depth of the *plateau* at 10 months was 1.2 mm. It appears from these data that after the density *plateau* reaches the maximum saturation density, its leading edge continues to move into the composite at a rate dependent on the square root of time.

Figure 37 shows the results of the same procedure for the type NC-775 composite at 75°C. In this case the maximum density was 1.10 g/cm^3 at a depth of penetration for the density *plateau* of 0.6 mm and a diffusivity of 4.5×10^{-5} mm^2/h.

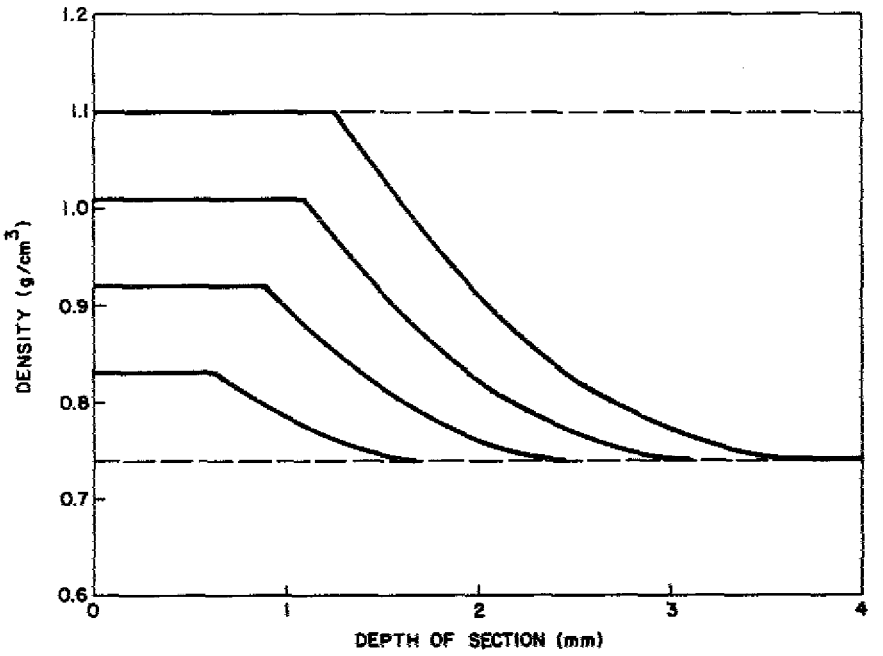

Fig. 35 — Idealized depth of penetration curves for DC-100 exposed to castor oil at 75°C for 3, 6, 9, and 12 months (bottom to top curves, respectively)

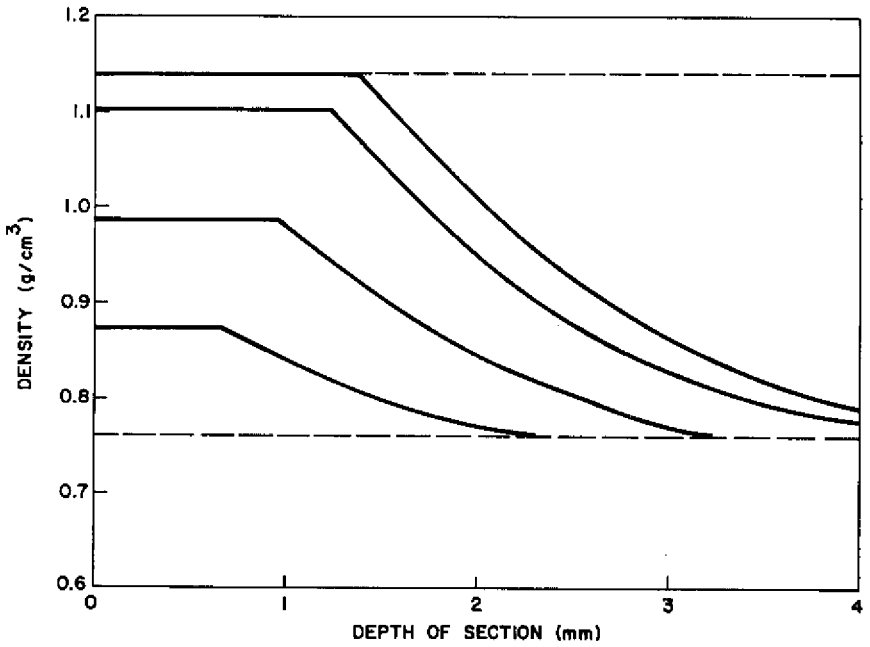

Fig. 36 — Idealized depth of penetration curves for DC-116 exposed to castor oil at 75°C for 3, 6, 9, and 12 months (bottom to top curves, respectively)

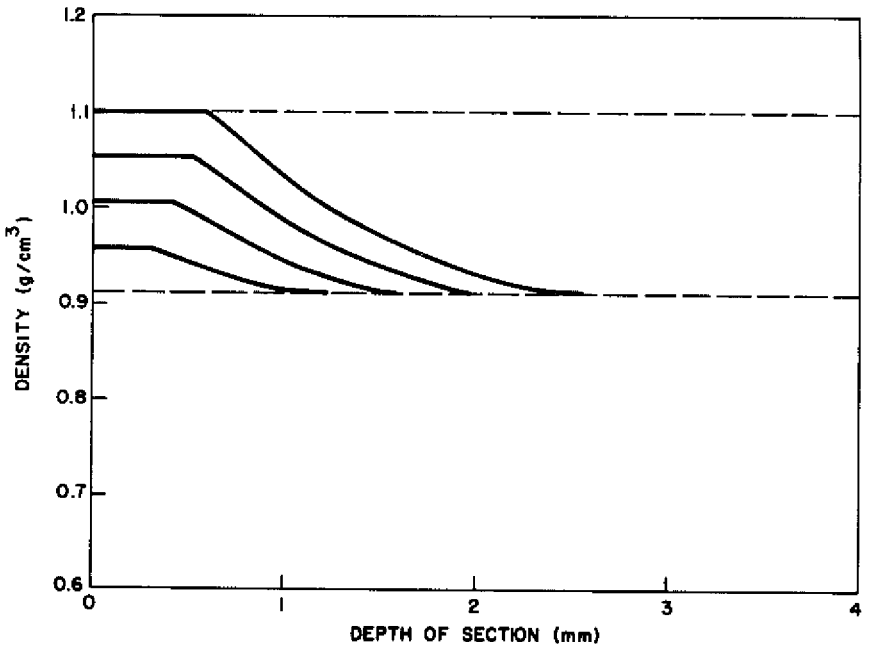

Fig. 37 — Idealized depth of penetration curves for NC-775 exposed to castor oil at 75°C for 3, 6, 9, and 12 months (bottom to top curves, respectively)

The type NC-710 composite does not seem to follow the same pattern. Although each individual curve does resemble the general shape expected, there is no regularity to the density *plateau*. The reason for this inconsistency is evident from microscopic observation of sections cut at right angle to the direction of flow. There it can be seen that the castor oil penetrates the type NC-710 in individual castor oil *channels* rather than as a uniform liquid front. In contrast, microscopic observation of sections from the other composite materials shows a uniform change in color with depth. No physical reason for the unique mode of permeation in the NC-710 is obvious at this time.

The type LC-800 composite could not be obtained in thickness sufficient for microtome sectioning, but some observations can be made from working with it. After 1 year at 75°C, the castor oil did not appear to have progressed past the outer layer of the exposed cork granules. Although this unfortunately cannot be quantified, it appears that silicone rubber has an extremely small diffusion constant when immersed in castor oil.

The castor-oil penetration process in cork-rubber composites is a threefold one. First, the castor oil flows relatively fast into the exposed individual cork granules, illustrated in Fig. 38. From these cork granules, it then diffuses in the direction of the decreasing castor-oil gradient, which can actually be in any direction as illustrated by Fig. 39. This produces an area of relatively constant density for a distance into the composite governed by the size of the largest cork granules. Complete saturation in this area is dependent on the size of the cork granules, the percent cork by volume, and the diffusivitive of the particular rubber used in the composite. Beyond this density *plateau*, the castor oil penetrates at a rate controlled by the diffusion rate of the rubber matrix (Fig. 40).

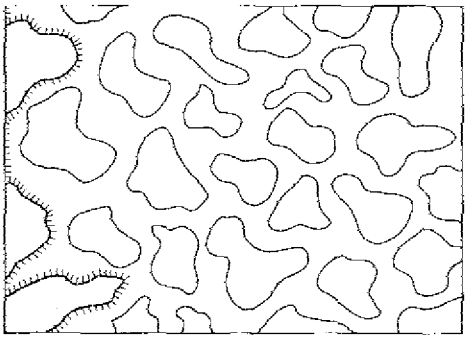

Fig. 38 — The early stage of permeation with castor-oil flow through the exposed cork granules dominating, with a slight influence of diffusion

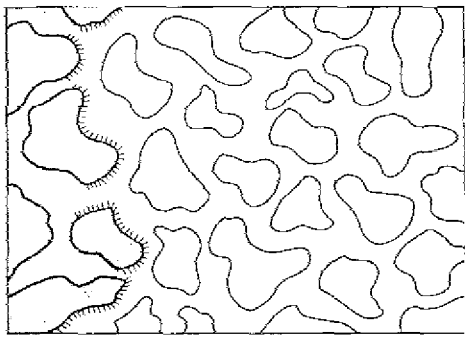

Fig. 39 — The intermediate stage of permeation with a combination of castor oil flow and diffusion

Fig. 40 — The advanced stage of castor-oil permeation with diffusion through the rubber matrix as the controlling factor

Acoustic Impedance Tube

Inspection of the sound-speed and attenuation graphs (Figs. 24 through 28) obtained from the acoustic impedance tube reveals the type of behavior generally expected of cork-rubber composites. The materials have low sound speeds with high attenuations at low hydrostatic pressures with increasing sound speeds and decreasing attenuations as the pressure is increased. This is because the material goes from a cork-dominated composite to a rubber-dominated material as the cork granules are compressed by the higher pressures.

More importantly for this investigation, the graphs show that the sound-speed and attenuation curves are very similar for unsoaked samples but they vary significantly in the castor-oil-soaked samples. Figures 24 and 25 show a very large increase in the sound speed for soaked composites DC-100 and DC-116, especially at low pressures. Composite NC-710 appears to have a slightly smaller sound-speed increase compared to that of the types DC-100 or DC-116. Type NC-775 exhibits a greatly reduced increase in sound speed, but type LC-800 has the smallest increase. A similar pattern for the decrease in attenuation is also evident. Table 16 shows that there is an approximate relationship between the amount of castor oil absorbed by the composite and the increase in the speed of sound in the material.

Combining this information with that from the microtome sectioning gives a satisfactory explanation. The DC-100 and DC-116 samples of 0.318-cm thickness are in effect completely saturated after soaking in castor oil at 75°C for a year; therefore, an increase in hydrostatic pressure would

Table 16 — Percentage Increase in Weight and Sound Speed (at 0-MPa pressure) for Five Cork-Rubber Composites Exposed to Castor Oil at 75°C for 1 Year

Cork-Rubber Material	% Increase in Weight	% Increase in Sound Speed
DC-116	68	210
DC-100	65	198
NC-710	50	123
NC-775	13	62
LC-800	9	25

distort the entire sample uniformly with very little volume change. On the other hand, the NC-775 and LC-800 samples, because of their small rates of diffusion and small cork granule size, have unsoaked material sandwiched between their outer layers of the castor-oil-soaked material. Thus, with increasing hydrostatic pressure, the inner dry portion is compressed by a greater percent than the outer edges. The type NC-710 acts somewhat as a combination of the completely saturated material and the castor-oil-layered material because of the *castor-oil channel effect.*

G19 Hydrophone Calibrator

The results shown in Figs. 30 through 34 are the tests in which a PZT-4 disc was radially wrapped with the various cork-rubber composites of 0.318-cm thickness and tested for voltage sensitivity in the G19 calibrator. The material was then replaced by another piece of the same material that had been exposed to castor oil at 75°C for a year. The drop in voltage sensitivity at the low-frequency end of the curves is low-frequency rolloff caused by the liquid medium (in this case Flourinert 75) seeping into the interspace between the pressure-release material and the PZT-4 element. The apparent dip in sensitivity at 900 Hz was caused by the error produced by a very high voltage reading from the F61 hydrophone due to resonance in the calibrator.

The relationship between castor-oil content and loss of hydrophone sensitivity of all test samples is best shown in tabular form. It should be noted that the pressure-release characteristics of all materials tested were very close before being exposed to castor oil. Table 17 shows the materials listed in order of decreasing castor-oil absorption. With the exception of composite DC-100, this is the same order as that of decreasing loss of hydrophone sensitivity. The voltage sensitivity comparisons were done at 700 Hz because the curves were very stable in this region.

Possibly the most striking way to show the effect of loss in sensitivity is by an overlay of Figs. 29, 30, and 34, as shown in Fig. 41. This shows a drastic difference in the acoustic insulating ability of types DC-100 and LC-800 after 1 year in castor oil at 75°C.

These results might have been anticipated from the impedance-tube work previously discussed, which showed that composite DC-100 almost doubles in sound speed at 0 MPa while the sound speed of LC-800 changes by only 25% after castor oil soaking.

Table 17 — Percentage Increase in Weight and Loss of Sensitivity (at 700 Hz) for Five *Cork-Rubber Composites* Exposed to Castor Oil at 75°C for 1 Year

Cork-Rubber Material	% Increase in Weight	Loss of Sensitivity (dB)
DC-116	68	9.9
DC-100	65	11.5
NC-710	50	4.1
NC-775	13	3.7
LC-800	9	0.2

The rate of change in the voltage sensitivity of a hydrophone can be calculated by including an appropriate term in Eq. (12) to allow for aging of a decoupling material. Equation (12) then becomes

$$M = \left\{ 2 \left[f(\rho_1, \rho_2, c_1, c_2) \right] g_{31} + g_{33} \right\} x \, . \tag{21}$$

Although the form of dependency is complex, simplifying assumptions from plane-wave acoustics gives

$$f(\rho_1, \rho_2, c_1, c_2) = 1 - \frac{\rho_1 c_1 - \rho_2 c_2}{\rho_1 c_1 + \rho_2 c_2} \, . \tag{22}$$

If the values for sound speed and density of the DC-100 samples and the Fluorinert 75 used in the G19 calibrator are substituted into Eq. (21) with the plane-wave function, the following results are obtained for dry DC-100:

Fluorinert 75: $\rho_1 = 1.76$ g/cm^3
$c_1 = 656$ m/s

DC-100: $\rho_2 = 0.74$ g/cm^3
$c_2 = 300$ m/s
$M = 0.0181x$.

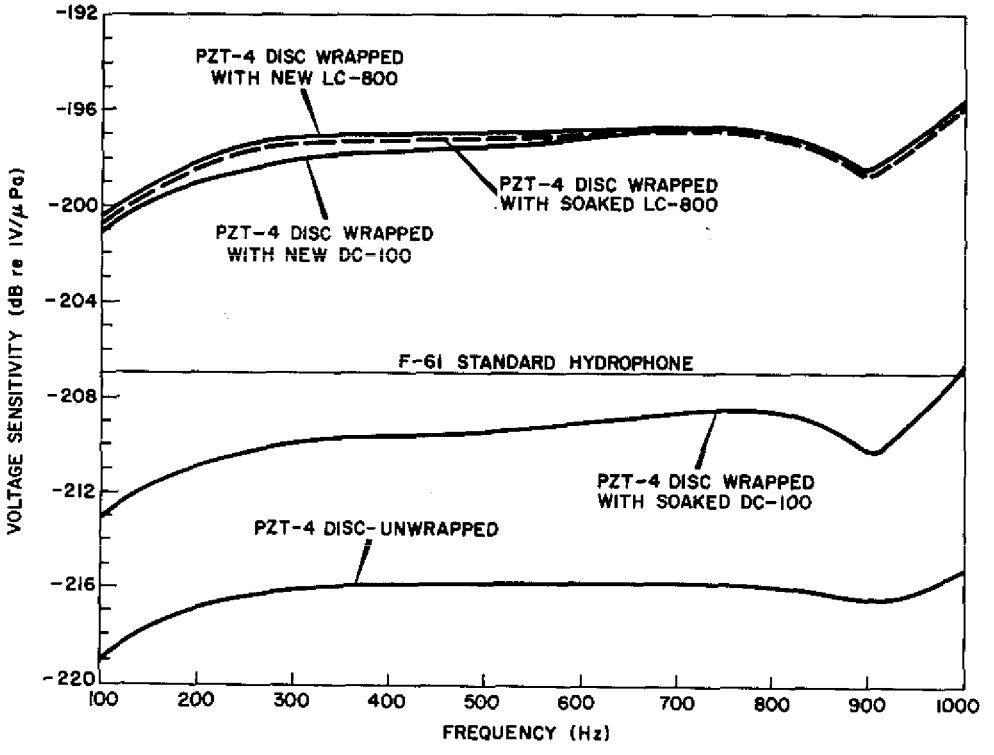

Fig. 41 — Comparison of the degradation in hydrophone sensitivity caused by soaking DC-100 and LC-800 in castor oil at 75°C for a year

For castor-oil-soaked composite DC-100 they are:

$$\rho_2 = 1.10 \text{ g/cm}^3,$$
$$c_2 = 1000 \text{ m/s},$$
$$M = 0.0042x,$$

or a change in sensitivity of a hydrophone element of −12.7 dB. This compares favorably to the change in sensitivity found with the G19 calibrator under the same conditions of −11.5 dB. Table 18 compares the predicted loss in sensitivity of the test hydrophone with the actual loss in sensitivity as presented in Table 17. In all cases the predicted values are within experimental error of the test values and the variations expected from the assumptions of Eq. (22).

The temptation at this point is to write equations to calculate the acoustic properties of the cork-rubber composite during the period between it being a dry material and it being a completely soaked material. The density of the sample in bulk can certainly be calculated from the parameters in Table 15 and the time and temperature of exposure. If next we assume that the change in sound speed is proportional to the change in density, the sound speed may be determined at any time and temperature. However, the analysis breaks down when one tries to use the density times sound speed (acoustic impedance) at intermedidate times to calculate the acoustic reflections, because this impedance value is an average for the bulk of the sample. Since the oil is penetrating the composite material along a front, the use of an average acoustic impedance is invalid. This deficiency is borne out by the practical observation that even a very thin layer of cork-rubber composite will effectively shield a hydrophone element. The important thing then would be to calculate the time necessary for the edge of the fluid front to reach the inside face of the shielding composite. Until that time, the sensitivity of the element would be essentially unchanged. After that time, the sensitivity would decrease in some relation to the acoustic impedance of the innermost layer of composite.

Table 18 — Loss in Sensitivity of a PZT-4 Test Hydrophone After Dry Acoustical Shielding Has Been Replaced by Castor-Oil-Soaked Pressure-Release Material Compared to the Calculated Loss in Sensitivity

Cork-Rubber Material	G19 Results (dB)	Calculated Loss in Sensitivity (dB)
DC-100	−11.5	−12.7
DC-116	−9.9	−11.7
NC-710	−4.1	−6.8
NC-775	−3.7	−3.4
LC-800	−0.2	−1.0

CONCLUSIONS

The conclusions of this study must be tempered by the fact that the analyses were, of necessity, performed on samples from a single batch of each type of material. These materials have a history of poor repeatability and, therefore, should be studied further.

The acoustic decoupling properties of cork-rubber composites are excellent before transducer fill-fluid saturation. This decoupling ability is greatly reduced with fluid absorption; therefore, the absorption mechanism must be understood. This investigation found the absorption mechanism to be a three-part one. First, the liquid flows into the exposed cork granules. Second, the liquid diffuses into the surrounding rubber matrix at a relatively slow rate. The third step is a combination of these with liquid flowing through the inner cork granules, but at a greatly reduced rate due to the limiting effect of the diffusion through the rubber matrix.

Next, this absorption rate must be predictable. The absorption rate was found to be described by a two-section graph, consisting of a density *plateau* region and a smoothly decreasing region that follows the error function. Given a unit time t_u (i.e., the time needed for the density *plateau* to reach a fully saturated state) and a unit distance d_u (i.e., the distance the density *plateau* extends into the material at t_u), the height of the density *plateau* for any time t can be determined from

$$(t/t_u)(\rho_{max} - \rho_{min}) = \rho_{plat} \tag{23}$$

if $t \leqslant t_u$ or $\rho_{max} = \rho_{plat}$ if $t > t_u$, where ρ_{max} is the density of saturated material, ρ_{min} is the density of dry material, and ρ_{plat} is the density of the material at time t. The distance x_{plat} that the density *plateau* extends into the material, at time t, can be determined from

$$d_u(t/t_u)^{1/2} = x_{plat} .$$

Beyond the density *plateau* the density with depth of penetration follows the error function as in Eq. (17).

The analysis above, along with the results of the gravimetric analysis, allows conclusions to be drawn about the usefulness of the various cork-rubber composites. The above techniques show that although the composite DC-100 is an excellent pressure-release material when dry, it loses this ability rather quickly when compared to some of the other composites tested.

Composite DC-116 has acoustic properties similar to those of the DC-100, but it absorbs castor oil at a faster rate. Thus, it is not a useful replacement for type DC-100.

The acoustic decoupling properties of composite NC-710 were again very similar to those of the DC-100, but the castor oil absorption mechanism is somewhat unpredictable. The castor-oil-absorption rate is similar to that of the DC-100, but the castor oil moves through the rubber matrix as *fingers* or channels rather than as a uniform liquid front.

A possible replacement for the DC-100 is composite NC-775. Its acoustic properties are as good as those of the DC-100 but they change more slowly with time, due to the slower castor-oil-absorption rate, and they are predictable. The only problem was that castor-oil surface blisters formed, but this was observed only at higher temperatures.

The best possible replacement for the DC-100 exposed to castor oil appears to be type LC-800. It has excellent acoustic decoupling properties and the slowest rate of castor-oil absorption. The drawbacks to this type are that it is over five times as expensive as the other composites and there may be a problem bonding a silicone rubber composite to other transducer components.

Further research is planned to allow quantitative calculation of the rate of degradation of a shielded ceramic element due to soaking of the cork-rubber composite material. This research will take the form of mathematical modeling of the decoupling process and measurements to determine more exactly the progress of the oil front through the material as a function of time and temperature.

ACKNOWLEDGMENTS

This research was a part of the Sonar Transducer Reliability Improvement Program, which is sponsored by the Naval Sea Systems Command Code 63X5 and managed by R. W. Timme. The authors would like to thank Dr. Timme and Dr. Pieter S. Dubbelday for their invaluable assistance during the course of this research.

REFERENCES

1. "Material Specifications," Armstrong Cork Co., Lancaster Pa., 1976.
2. "Design and Construction of Crystal Transducers," Summary Technical Report of Division 6, NDRC, Vol. 12, Washington, D.C., 1946.
3. R. W. Higgs and L. J. Ericksson, "Acoustic Decoupling Properties of Onionskin Paper," J. Acoust. Soc. Am. **46**, No. 1 (Part 2), 211-215, July 1969.
4. R. W. Higgs, P. M. D'Amico, and C. J. Speerschneider, "The Acoustical and Mechanical Properties of Sonite," J. Acoust. Soc. Am. **50**, No. 3 (Part 2), 946-954, September 1971.
5. R. W. Higgs and L. J. Eriksson, "Acoustic Decoupling Properties of Corprene DC-100," J. Acoust. Soc. Am. **46**, No. 5 (Part 2), 1254-1258, November 1969.
6. Morris L. Robertson, "A Letter Report on the DT-299/AQS-13 Hydrophone Stave Aging Problem Investigation," private communication, 20 October 1975.
7. M. E. Fife, "Cause of Aging in AQS-13B Hydrophone Element," Report No. 8920-R 285, private communication, The Bendix Corp., N. Hollywood, Calif., May 1976.
8. Warren P. Mason, *Physical Acoustics*, Vol. 1, Part A (New York, Academic Press, 1964).
9. Gerald A. Sabin, "Acoustic-Impedance Measurements at High Hydrostatic Pressures," J. Acoust. Soc. Am. **40**, No. 6, 1345-1353, 1966.
10. I. D. Groves, "Twenty Years of Underwater Electroacoustic Standards," NRL Report 7735, February 1974.
11. Robert E. Reed-Hill, *Physical Metallurgy Principles* (Princeton, N.J., D. Van Nostrand Co., Inc., 1964).

Appendix A

DIFFUSION EQUATIONS

Fick's first law of diffusion states

$$q' = -\widetilde{D}(\partial N/\partial x)\,, \tag{A1}$$

where $\widetilde{D}$ = diffusivity,
N = concentration,
q' = one-dimensional flux.

Combining this with conservation of mass in the form

$$(\partial q/\partial x) + (\partial N/\partial t) = 0 \tag{A2}$$

produces the diffusion equation (Fick's second law)

$$(\partial N/\partial t) = \widetilde{D}(\partial^2 N/\partial x^2)\,. \tag{A3}$$

The solution to Eq. (A3) under the boundary conditions that at the fluid-solid interface there is an inexhaustible supply of fluid and at $t = 0$ there has been no fluid permeation into the solid is

$$N = N_0\,\left[\,1 - \mathrm{erf}\,(x/2(\widetilde{D}t)^{1/2})\,\right]\,, \tag{A4}$$

where the error function erf is given by

$$\mathrm{erf}(s) = (2/\pi^{1/2})\int_0^S \exp\,(-t^2)\,dt\,. \tag{A5}$$

Therefore the flux through Eq. (A1) is

$$q' = -\widetilde{D}(\partial N/\partial x) = (N_0/(\pi\widetilde{D}t)^{1/2}\exp\,(-x^2/4\widetilde{D}t)\,. \tag{A6}$$

The measured quantity in this investigation was total absorbed weight per unit area, which is actually the integrated flux. This is equal to

$$\int_0^\infty N(x,t)\,dx\,. \tag{A7}$$

Since Eq. (A2) gives

$$\int_0^\infty (\partial q'/\partial x)\,dx + (\partial/\partial t)\int_0^\infty N(x,t)\,d\,(x) = 0 \tag{A8}$$

and

$$q'(\infty) = 0\ , \tag{A9}$$

then

$$q'(0,t) = (\partial/\partial t)\int_0^\infty N(x,t)\,dx \tag{A10}$$

and

$$\int_0^\infty N(x,t)\,dx = \text{weight/area}, \tag{A11}$$

$$= \int_0^t q'(0,t)\,dt\ , \tag{A12}$$

$$= \int_0^t (N_0/(\pi\widetilde{D}t)^{1/2})\,dt\ , \tag{A13}$$

$$= (N_0/(\pi\widetilde{D})^{1/2})\ t^{1/2}\ . \tag{A14}$$

Therefore,

$$\text{measured weight/area} = (N_0/(\pi\widetilde{D})^{1/2})\ t^{1/2}\ . \tag{A15}$$

As seen in Eq. (A15) a log-log plot of the integrated liquid flux vs time will have a slope of 0.5 (note the $t^{1/2}$ dependence).

Appendix B

DERIVATION OF THE IMPEDANCE-TUBE EQUATIONS

The measurement method is based on the analogy between an electrical and an acoustical transmission line. Plane-wave propagation is assumed and is attained in practice by using a rigid-walled tube with a diameter much smaller than the wavelength of sound in either the water or in the test material. Information obtained on materials placed in the tube may be used to determine the complex propagation constant γ and the characteristic acoustic impedance Z_0 of the materials. Other acoustic properties of the material may then be determined from γ and Z_0.

The characteristic acoustic impedance Z_0 of viscoelastic materials like corprene is

$$Z_0 = j\omega\rho/\gamma \,, \tag{B1}$$

where ρ is material density, ω is angular frequency, and $\gamma = (\alpha + jk')$ is the complex propagation constant with α being the attenuation and k' the wave number.

The input impedance of a sample of length x, terminated by a rigid boundary is given by the expression

$$Z_{in} = Z_0 \coth(\gamma x) \,. \tag{B2}$$

The complex reflection coefficient r, at a plane fluid-solid interface is

$$r = (Z_{in} - Z_T)/(Z_{in} + Z_T) \,, \tag{B3}$$

where Z_T is the characteristic acoustic impedance of the fluid medium, which is water in most instances. Therefore, the complex reflection coefficient for the sound pressure represents an indirect measurement of the water-to-sample boundary input impedance given by

$$Z_{in}/Z_T = (1 + r)/(1 - r) \,. \tag{B4}$$

If this indirect relation for the sample input impedance is substituted into a normalized relation for the input impedance of a sample backed by a rigid boundary, Eq. (B2), then the resultant relationship between reflection coefficieint and characteristic acoustic impedance of the sample is

$$(1 + r)/(1 - r) = (Z_0/Z_T) \coth(\gamma x) \,. \tag{B5}$$

Substitution of the characteristic acoustic impedance of viscoelastic material, Eq. (B1), for Z_0 in Eq. (B5) results in the expression

$$Z_0/Z_T = j\left[\omega\rho/\rho_T c_T(\alpha + jk')\right] \,, \tag{B6}$$

where $Z_T = \rho_T c_T$ is the characteristic acoustic impedance of water. Replacing the ratio Z_0/Z_T in Eq. (B5) with the right-hand side of Eq. (B6) yields

$$(1 + r)/(1 - r) = j \left[\omega\rho/\rho_T c_T(\alpha + jk')\right] \coth \left[(\alpha + jk')\, x\right] \tag{B7}$$

or

$$\left[(1 + r)/(1 - r)\right] \left[1/(\rho/\rho_T)k_T\right] = j \left[1/(\alpha + jk')\right] \coth \left[(\alpha + jk')x\right]. \tag{B8}$$

Equation (B8) may be used to determine α and k', the components of the complex propagation constant γ, for the sample material. The values of the left-hand side of Eq. (B8) are all experimentally measured quantities. The quantity r is the complex reflection coefficient, ρ/ρ_T is the ratio of sample density to the density of water, and $k_T = \omega/c_T$, where c_T is the speed of sound in water.

Equation (B8) is a transcendental equation that cannot be solved for unknown values of α and k' algebraically. An iterative computer program (Appendix C) has been developed that will calculate the right-hand side of Eq. (B8). Starting with arbitrary values of α and k', the program computes and compares a value for the left-hand side of the equation with the measured value. The values of α and k' are then incremented or decremented until the equation is satisfied within a specified tolerance.

Appendix C

COMPUTER PROGRAM FOR IMPEDANCE-TUBE DATA

The following is a FORTRAN program developed at NRL-USRD to calculate sound speed and attenuation of materials tested in the acoustic impedance tube.

```
      CALL ERRSET(63,,.FALSE.,,,.FALSE.,,)
      CALL ERRSET(64,,.FALSE.,,,.FALSE.,,)
      WRITE(6,903)
903   FORMAT(//,' INPUT:SAMPLE LENGTH(CM),DENSITY(GM/CC),STARTING AT',
     1'TENUATION(DB/M), AND STARTING SOUND SPEED (M/SEC)')
      READ(5,900) DIST,DENS,ALFA,C
3     WRITE (6,904)
 904  FORMAT (' INPUT: PRESSURE (KPSI),FREQUENCY(KHZ),RX,THX,RS,THS')
      READ(5,901,END=200) PRES,FKHZ,RX,THX,RS,THS
      RHOM=RX/RS
900   FORMAT(4F10.0)
901   FORMAT(6F10.0)
      IF(THS-180.) 80,80,90
80    IF(THX-THS-180.)100,100,110
90    IF(THX-THS+180.)120,100,100
100   TH2M=THX-THS
      GO TO 9
110   TH2M=THX-THS+360.
      GO TO 9
120   TH2M=THX-THS-360.
9     FREQ=FKHZ*1000.
      I=0
      J=0
19    I=I+1
      TAFD=.230259E-02*ALFA*DIST
      TWKD=.125664*FREQ*DIST/C
      CHAD=EXP(TAFD)+EXP(-TAFD)
      FMAG=SQRT((CHAD+2.*COS(TWKD))/(CHAD-2.*COS(TWKD)))
      A=TWKD/TAFD
      ZMAG=DENS*C*FMAG*SQRT(A*A/(A*A+1.))/(1460.+10.*PRES)
      SOSH=2.*SIN(TWKD)/(EXP(TAFD)-EXP(-TAFD))
      ZANG=ATAN(1./A)-ATAN(SOSH)
      RHOC=SQRT((ZMAG*ZMAG+1.-2.*ZMAG*COS(ZANG))/(ZMAG*ZMAG+
     1        1.+2.*ZMAG*COS(ZANG)))
      TH=ATAN(2.*ZMAG*SIN(ZANG)/(ZMAG*ZMAG-1.))
      IF(ZMAG-1.) 6,8,8
6     TH=3.14159+TH
8     THDG=TH*57.2958
      TKTD=7.2*FREQ*DIST/(1460.+10.*PRES)
      TH2=THDG+TKTD
20    IF(TH2-180.)23,23,22
22    TH2=TH2-360.
      GO TO 20
23    IF(I-1)25,25,29
29    RHO=RHOC-RHOM
      IF(RHO*RHO)39,25,25
25    RHO=RHOC-RHOM
      IF(RHO)30,39,31
30    RHO=-RHO
31    IF(RHO-.005)39,39,32
32    RHO=RHOC-RHOM
      IF(RHO)11,39,10
10    ALFA=ALFA+.2
```

```
--
        J=0
        GO TO 19
11      ALFA=ALFA-.2
        IF(ALFA-.1)60,60,61
60      ALFA=.01
61      J=0
        GO TO 19
39      J=J+1
        IF(J-1)85,85,40
40      THIA=TH2-TH2M
        IF(THIA*THTA)24,85,85



85      THTA=TH2-TH2M
        IF(THTA)41,24,42
41      THTA=-THTA
42      IF(THTA-.5)24,24,43
43      THTA=TH2-TH2M
        I=0
        IF(THTA)17,24,16
16      C=C-10.
        GO TO 19
17      C=C+10.
        GO TO 19
24      WRITE(6,902) ALFA,C,RHOM,TH2M,RHOC,TH2
902     FORMAT(//,' ATTENUATION =',F7.2,'DB/M',/,' SOUND SPEED=',F5.0,'M',
        1'/SEC',/,20X,'REFLECTION COEFFICIENT',20X,'PHASE ANGLE',/,' ME',
        2'ASURED',16X,E13.6,20X,F15.4,/,' CALCULATED',14X,E13.6,20X,F15.4)
        GO TO 3
200     CALL EXIT
        END
```